Universidade de Aveiro Departamento de Química
Ano 2015

Mafalda Alves Fernandes Bispo

Galacto-ftalocianinas de silício para o tratamento do cancro da bexiga

Galacto-silicon phthalocyanines for bladder cancer treatment

Universidade de Aveiro Departamento de Química
Ano 2015

Mafalda Alves Fernandes Bispo

Galacto-ftalocianinas de silício para o tratamento do cancro da bexiga

Galacto-silicon phthalocyanines for bladder cancer treatment

Dissertação apresentada à Universidade de Aveiro para cumprimento dos requisitos necessários à obtenção do grau de Mestre em Bioquímica, ramo da Bioquímica Clínica, realizada sob a orientação científica do Doutor João Tomé, Investigador Principal do Departamento de Química da Universidade de Aveiro, do Professor Tomás Torres Cebada, Professor Catedrático da Universidade Autónoma de Madrid e da Doutora Rosa Fernandes, Investigadora Auxiliar do Instituto de Imagem Biomédica de Luz e Imagem (IBILI) da Faculdade de Medicina da Universidade de Coimbra.

Dedico esta tese a todos aqueles que sempre acreditaram em mim.

o júri

presidente

Professor Doutor Pedro Miguel Dimas Neves Domingues
Professor Auxiliar c/ Agregação do Departamento de Química da Universidade de Aveiro

Doutor Flávio Nelson Fernandes Reis
Investigador auxiliar da Faculdade de Medicina da Universidade de Coimbra

Doutor João Paulo Costa Tomé
Investigador Principal do Departamento de Química da Universidade de Aveiro

agradecimentos

Ao meu orientador Doutor João Tomé por ter acreditado em mim desde o projeto de licenciatura e por ter-me realizado a vontade de fazer parte da tese de mestrado em Madrid. Obrigada também por toda a orientação científica.
À minha co-orientadora Dra Rosa Fernandes, por me ter recebido sempre bem no laboratório do IBILI e por ser sempre prestável quando preciso.
Ao meu co-orientador Professor Tomás Torres, por me ter recebido tão bem em Madrid e me ter feito sentir logo parte do grupo. Obrigada por acreditar em mim e por me ter dado a possibilidade de ficar os 4 meses no seu grupo.
À Patrícia Pereira por me fazer gostar cada vez mais do meu trabalho com a paixão que sempre põe nas coisas que faz. Obrigada também por teres sido sempre incansável e amiga nestes últimos três anos que trabalhamos juntas.
To Venkat, for always saving me in the organic chemistry lab when I was in trouble and for his friendship.
Ao Tiago, por ser a minha alma gémea, por dizer sempre as palavras certas no momento certo, pela cumplicidade, pelo carinho e mais importante pela paciência e confiança que depositas em mim!
Aos meus pais por terem possibilitado a minha ida a Madrid, algo que eu sempre quis, por me darem a oportunidade de ter uma boa formação e por me apoiarem em todos os momentos da minha vida. Obrigada por todo o carinho, paciência, palavras sábias e alento. Todo o meu esforço é no sentido de vos deixar orgulhosos de forma a retribuir-vos de alguma forma todo o esforço que fizeram para me darem a vida que tenho hoje.
Á minha avó, aos meus tios e à minha Joaninha por acreditarem nas minhas capacidades e por festejarem as minhas vitórias com orgulho.
Aos meus amigos, que aturaram o meu mau feitio ao longo deste ano cheio de aventuras e que sempre acreditaram que eu iria conseguir fazer tudo, mesmo andando de um lado para o outro. Obrigada por estarem sempre presentes em todas as minhas conquistas, com palavras de conforto e amigas que me puxam sempre para cima.

A Francesca, mi guapi, por haberme recibido tan bien en el laboratorio, por la amistad que hemos creado y por siempre pensar en positivo cuando las cosas no iban tan bien.
Al Profesor Salomé Rodriguez, por la buena disposición en el laboratorio, por la disponibilidad en ayudarme siempre con los espectros de RMN que tantos dolores de cabeza nos dieron.
A mis amigos del 3º piso del departamento de química orgánica por todos los momentos vividos, toda la risa, todas las pausas que hacíamos solo porque no teníamos ganas de trabajar (mucho) y por hacerme sentir como en casa.

Palavras-chave Terapia Fotodinâmica, Cancro da Bexiga, Ftalocianinas de silício, Galectinas, Unidades galacto-dendríticas

Resumo

A terapia fotodinâmica (*PhotodynamicTherapy*, PDT) é uma metodologia emergente no tratamento de diversas doenças oncológicas e tem por base o uso de oxigénio molecular, luz e um fotossensibilizador (FS) para seletivamente destruir as células tumorais. Em oncologia, a PDT leva à indução de espécies reativas de oxigénio (*reactive oxygen species,* ROS) no tecido tumoral, no qual ocorreu previamente o *uptake* preferencial e/ou a retenção de um FS.

As ftalocianinas têm-se vindo a revelar FSs promissores na PDT devido às suas propriedades foto-físicas. Contudo, estes compostos para além de pouco solúveis em água, têm problemas de agregação e de especificidade para os tecidos tumorais. Assim, o trabalho apresentado nesta tese teve como objetivo principal conjugar co-axialmente ftalocianinas de silício (*silicon phthalocyanines*, SiPcs) com duas moléculas de galactose (**SiPcGal$_2$**) e com duas unidades dendríticas de galactose (**SiPcGal$_4$**) para que estes FSs fossem reconhecidos por galectinas (*e.g.* galectina-1) sobrexpressas em células tumorais. Contudo, os compostos desejados finais não foram obtidos, uma vez que a remoção dos grupos isopropilideno, protetores dos grupos hidroxilo das unidades de galactose, não foi conseguida. Assim, foram avaliadas as propriedades foto-físicas e foto-químicas das SiPcs com as galactoses protegidas, comparando com a SiPc dihidróxido (**SiPc(OH)$_2$**), de forma a estudar a influência da conjugação co-axial de biomoléculas no core destes tipo de FSs. Infelizmente, a solubilidade das SiPcs em solventes aquosos não foi conseguida, contudo o seu espectro de absorção UV-visível evidenciou elevada absorção a altos comprimentos de onda (650-700 nm), janela espectrofotométrica onde ocorre uma penetração mais profunda da luz nos tecidos. Para além disso, estes FSs demonstraram-se excelentes marcadores fluorescentes, estáveis após irradiação e bons geradores de $^1O_2$. Foram ainda realizados estudos *in vitro* com o objetivo de validar o seu potencial fotodinâmico no tratamento do cancro da bexiga, sendo que a **SiPcGal$_4$** e a **SiPcGal$_2$** agregaram nas células, tendo assim um baixo uptake, baixa toxicidade após foto-ativação e baixa produção de ROS.

No geral, as SiPcs demonstraram um grande potencial como futuros FSs para a PDT, dado as suas excelentes propriedades foto-físicas, o que nos incentiva na descoberta de novas técnicas que diminuam a sua agregação nas células, como a utilização de bio-formulações estáveis e a desproteção das moléculas de galactose, que também irá aumentar a sua especificidade para células tumorais.

Keywords Photodynamic Therapy, Bladder Cancer, Silicon Phthalocyanine, Galectins, Galacto-dendritic units

Abstract

Photodynamic Therapy (PDT) relies on the combination of a photosensitizer (PS), light and molecular oxygen (O_2) to generate reactive oxygen species (ROS), which can trigger cell death pathways. In oncology, the PS needs to be preferentially accumulated in cancer cells and a good generator of ROS (especially singlet oxygen, $^1O_2$).

Phthalocyanines (Pcs) are promising PSs in PDT due to their photochemical and photophysical properties. However, Pcs present solubility and aggregation problems, as well as low selectivity to the cancer tissue. Therefore, it will be conjugated a silicon phthalocyanine (SiPc) with two galactose molecules (**SiPcGal$_2$**) and another with two galacto-dendritic units (**SiPcGal$_4$**), both in axial positions. The aim of that conjugation is to promote the binding of the PS with galactose-binding proteins such as galectins (*e.g.* galectin-1) which are found to be overexpressed in cancer cells. Nevertheless, the desired compound were not obtained, once the hydrolysis of the isopropylidene galactose-protective groups didn't work. Thereby, the photophysical and photochemical properties of those two SiPcs with the galactose-protective groups were studied in comparison with the SiPc dihydroxide (**SiPc(OH)$_2$**), in order to study the SiPc core properties as well as the influence of an axial conjugation of biomolecules. The PSs solubility was compromised in an aqueous solution, however their absorption UV-Visible spectra showed high absorption peaks at a high wavelengths range (650–700 nm), which is the ideal therapeutical window where there is a higher penetration of light into the tissues. Furthermore, these SiPcs demonstrated to be good fluorescence labels, photostable and good $^1O_2$ generators. *In vitro* studies were performed with the aim of validating them as photodynamic therapeutic agents against bladder cancer cells, however **SiPcGal$_4$** and **SiPcGal$_2$** aggregated on cells, having a low uptake, phototoxicity and ROS production.

Overall, SiPcs have demonstrated a great potential as future PSs for PDT, thanks to their excellent photophysical properties, which prompt us in the discovery of different approaches that diminished their aggregation on cells, such as the incorporation of PSs into bio-stable formulations and the deprotection of the galactose molecules, which will also increase their specificity to tumoral cells.

Contents

Abbreviations and acronyms

ADME	Adsorption, distribution, metabolism and excretion
ASR	Age standardized incidence rate
BCG	Bacillus Calmette-Guerin
Acridine	2,3-benzoquinoline
BC	Bladder Cancer
BCA	Bicinchoninic Acid
BSA	Bovine Serum Albumin
TMSBr	Bromotrimethylsilane
CRD	Carbohydrate-recognition domains
CIS	Carcinoma *in situ*
ALA	Delta-aminolevulinic acid
DAPI	4’,6-diamino-2-phenylindole
H_2DCFDA	2’,7’-dichlorohydrofluorescin
DCM	Dichloromethane
DHE	Dihydroethidium
DIPEA	N,N-diisopropylethylamine
DMF	Dimethylformamide
DMSO	Dimethyl sulfoxide
MTT	3-(4,5-Dimethylthiazol-2-yl)-2,5-diphenyltetrazolium bromide
DPBF	1,3-Diphenylisobenzofuran
ESI^+-MS	Electrospray ionization mass spectrometry
EPR	Enhanced permeability and retention
FDA	Food and Drug Administration
Hp	Hematoporphyrin
HpD	Hematoporphyrin Derivative
HSA	Human Serum Albumin
IR	Infrared
RNAi	Interference Ribonucleic Acid
IC	Internal Conversion
ISC	Intersystem crossing
IM	Intramuscular
IV	Intravenous
LEDs	Light Emitting Diodes
MALDI-MS	Matrix-assisted laser desorption/ionization Mass Spectrometry
TPP	meso-tetraphenylporphyrin
MPcs	Metallo-phthalocyanines
MB	Methylene Blue
MitoPy1	Mitochondria peroxy yellow 1
mAb	Monoclonal antibody

NMR	Nuclear magnetic resonance
PK	Pharmacokinetics
PBS	Phosphate-buffered saline
P	Phosphorescence
PAPs	Photoactive porphyrins
PDT	Photodynamic Therapy
PS	Photosensitizer
Pc	Phthalocyanine
Por	Porphyrin
Pre-mRNA	Precursor messenger ribonucleic acid
PpIX	Protoporphyrin IX
ROS	Reactive Oxygen Species
rt	Room temperature
SiPc	Silicon phthalocyanine
SDS	Sodium dodecyl sulfate
SC	Subcutaneous
PFA	Paraformaldehyde
Rose Bengal	4,5,6,7-tetrachloro-2',4',5',7'-tetraiodofluorescein
THF	Tetrahydrofuran
TLC	Thin layer chromatography
TUR	Transurethral resection
TCT	2,4,6-trichloro-1,3,5-triazine
TNM	Tumor-Node-Metastases
UV/Vis	UV/Visible

CHAPTER I

INTRODUCTION

1. Overview

Cancer is a disease caused by an abnormal growth of cells which tend to proliferate in an uncontrolled way and, in some cases, to spread out to other organs of the body through the blood and lymph systems. This process is named metastasis and corresponds to the most advanced stage of cancer and the most common cause of cancer death. There are more than 100 different types of cancer. In 2012, there were approximately 14 million of new cancer cases and 8.2 million of cancer related deaths (1). The most common and conventional cancer treatments are surgery, and/or radiotherapy, and/or chemotherapy. However, there are serious side effects in those treatments, such as loss of normal cell function. In order to counter that, less invasive approaches were developed over the years, targeted therapies that use drugs to more precisely identify and destroy cancer cells, causing far less damage to healthy cells. Photodynamic Therapy (PDT) is a newer type of therapeutic approach that uses special drugs named photosensitizing agents, along with light to induce cancer cell death, through the production of reactive oxygen species (ROS). PDT can be applied alone or in combination with the aforementioned traditional treatments (2,3).

The pursuit of new photosensitizing agents for PDT is a lively research field. Those drugs should specifically accumulate in cancer tissues and have high production of ROS. The conjugation of galactose targeting moieties with a porphyrinoid-based drug is a valuable way to achieve a high local concentration of that drug in tumor tissues, since certain galectins (*i.e.* galectin-1 and galectin-3) are overexpressed on the target cells relatively to normal tissues (4).

2. Photodynamic therapy

In oncology, PDT is an emerging treatment modality able to treat many forms of cancer and other non-neoplastic diseases (5-7), being particularly interesting in the tumors that occur in cavities (such as bladder, esophagus or intestine). This methodology combines a photosensitizer (PS) with light of appropriate wavelength and molecular oxygen (O_2). None of these elements are toxic by themselves, however when combined they generate ROS that kill malignant cells by triggering a cascade of cytotoxic reactions (8). In order to allow that the knowledge of photosensitization can be rapidly applied in clinical practice, PDT requires the cooperation of chemists (*e.g.*, for synthesis of new PS), biologists (*e.g.*, for testing new substances), physicists (*e.g.*, for light dosimetry), and clinicians (*e.g.*, for the transfer from the lab bench to the clinical application).

2.1 Brief History

The first clinical use of PDT date back to 1903 when Tappeiner and Jesionek combined a topical application of eosin with white light to treat skin tumors, lupus and condylomata of female genitalia (9). After ten years, Meyer-Betz found out that porphyrins (Pors) act as photosensitizing agents in humans while injecting 200 mg of hematoporphyrin (Hp) in himself. (10). However, after sun light exposure there were side effects, such as severe pain and swelling confined to the light-exposed areas. Around the 1960's, Schwartz and Lipson described the tumor accumulation of Hp derivatives (HpD, a mixture of monomers, dimers and oligomers) as well as their use in tumors photodetection (11). Since these pioneering works, several compounds have been developed and tested. Among them, there is Photofrin®, the first PS approved for clinical PDT in the treatment of superficial bladder cancer in Canada and early lung and advanced esophageal cancers in The Netherlands and Japan (12). Considering the ideal properties of a PS, that will be explained further on detail, a wide range of synthetic or natural PSs have been studied, tested *in vivo* and *in vitro*, and some of them are currently in advanced stages of clinical trials.

Examples of new PSs are synthetic Pors (13), benzoporphyrins (14), chlorins (15), phthalocyanines (Pcs) (16), among others.

2.2 Molecular basis of PDT

Photophysics

PDT is based on the PS administration and after a preferential uptake and/or retention period the affected area is irradiated with light to induce photoreactions. Upon illumination with light of an appropriate wavelength, PS absorbs a photon leading to the formation of an electronically excited singlet state (^{1}PS*). However, this short-lived species can lose their energy and restore the ground state by emission of fluorescence or by internal conversion (IC, non-radiative transitions between two electronic states with the same spin multiplicity) with energy loss as heat. The singlet state ^{1}PS*, can also undergo the process known as intersystem crossing (ISC), leading to formation of the long-lived triplet excited state (^{3}PS*). The energy of ^{3}PS* can be dissipated (leading the PS to its ground state) through two main pathways: i) thermal decay, *i.e.* IC; or ii) by emission of light, namely phosphorescence (P). In **Figure 1.1** it is represented a modified Jablonski diagram that illustrates the electronic states of the PS and the transitions between them. ^{3}PS* usually has a lifetime in the microsecond range (typically > 0.5 µs), which is sufficient to enable interaction between the excited PS and surrounding biomolecules. Moreover, this state can induce cytotoxic effects by PDT through two kinds of reactions, defined as *Type I* and *Type II* photoreactions (17).

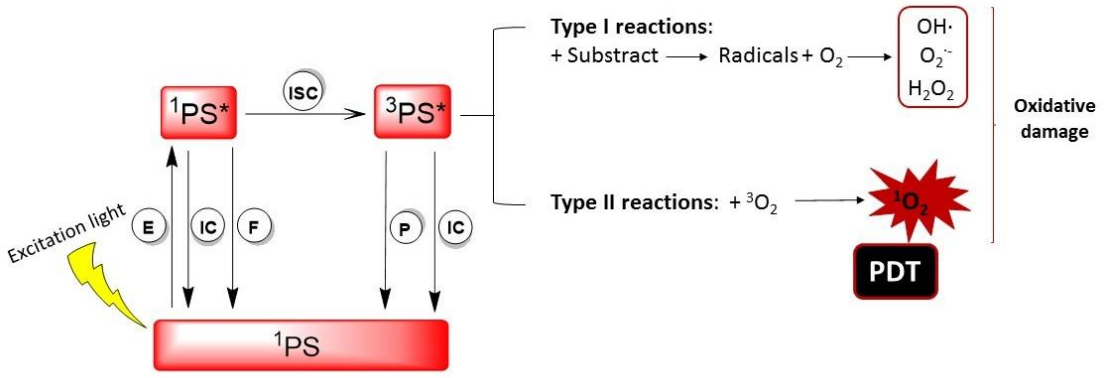

Figure 1.1 Modified Jablonsky energy diagram showing the various modes of excitation and relaxation occurring in PSs: excitation (E), internal conversion (IC), fluorescence (F), phosphorescence (P), intersystem crossing (ISC). *Type I* and *Type II* photoreactions are also represented.

Photochemistry

Type I photoreactions can proceed by an electron (and/or proton) transfer process, hence causing a direct interaction of $^3PS^*$ with the cellular substrate (lipids, proteins, nucleic acids, *etc.*) leading to generation of radicals. Subsequent reaction with O_2 forms ROS, such as the superoxide anion ($O_2^{\cdot-}$), the hydroxyl radical ($OH^{\cdot}$), and hydrogen peroxide (H_2O_2) that initiate radical chain reactions (18,19).

Alternatively, *Type II* photoreactions proceed by energy transfer, where the interaction of O_2 in its ground triplet state ($^3O_2$) with $^3PS^*$ generates a more reactive form of oxygen, *i.e.* singlet oxygen ($^1O_2$). This non-radical species are highly reactive towards electrons rich substrates such as for instance, double bonds, aromatic rings, amines and thioethers (18,19). They also react with plasmatic membrane biomolecules and different cellular organelles, leading to the selective destruction of the target cells by necrosis and/or apoptosis and/or autophagy-associated cell death, without damaging the healthy tissue (**Figure 1.1**). Antitumor effects of PDT derive from three inter-related mechanisms: direct cytotoxic effects on tumor cells, damage to the tumor vasculature and induction of a robust inflammatory reaction that can lead to the development of systemic immunity (3). The role of $^1O_2$ in the photodynamic effect is controversial between researchers. However, for most PSs

currently under investigation, the $^1O_2$-mediated photodynamic mechanism is the model of cytotoxic action usually accepted (20). To investigate the chemistry of $^1O_2$, several analytical tools can be used such as spectrophotometry, fluorimetry, and chemiluminometry. In spectrophotometry, $^1O_2$ react rapidly and irreversibly with a probe (*e.g.* diphenylisobenzofuran, DPBF) to initially yield an endoperoxide which, in turn, emerge into other products that do not fluoresce and have absorption spectra different from that of the probe (21). The use of selective and photo-activated PS makes PDT a promising technique for the treatment of a variety of oncological diseases.

3. Photosensitizers

A PS, which is a molecule that enters an excited state when exposed to light of a specific wavelength, can use that energy to induce cytotoxic reactions leading to cell death and tissue destruction. Thus, a good PS agent with potentially optimal properties for PDT should be endowed with specific features: i) single pure compound; ii) low manufacturing costs and good stability in storage; iii) no dark toxicity, but being toxic upon photo-activation; iv) rapid clearance from normal tissues to minimize phototoxic side effects; v) high triplet-state quantum yields, i.e., triplet-state with lifetimes enough and sufficiently energetic to produce $^1O_2$ and vi) high absorption peak between 600 and 800 nm (therapeutic window). This last characteristic is related to the aforementioned light penetration into the tissues once in this range the light wavelengths are still energetic enough to produce $^1O_2$ and tissues are more transparent, thus light has its maximum depth of penetration (**Figure 1.2)**. Absorption bands at shorter wavelengths than 600 nm have less tissue penetration due to the endogenous absorption by tissue cromophores (*e.g.* oxy-/deoxy- hemoglobin, melanin), leading to skin photosensitivity. At wavelengths higher than 800 nm there is not enough energy for the $^3PS^*$ transfer to the ground state of O_2 in order to excite it to the singlet state (20).

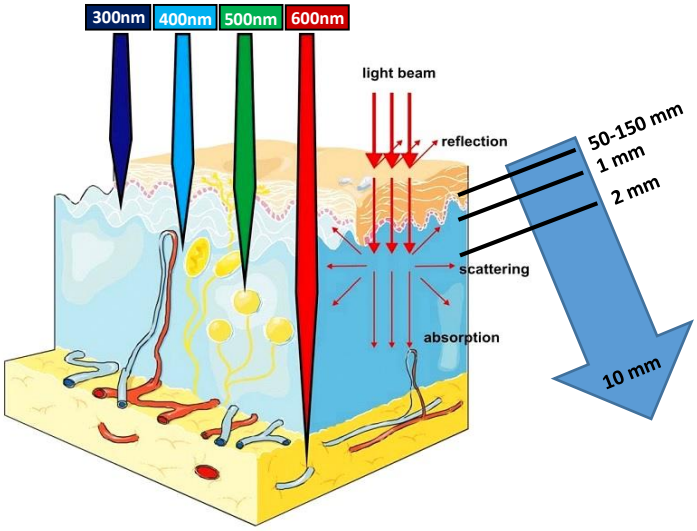

Figure 1.2. Propagation of light through the tissues. Adapted from (3).

Although many PSs, such as methylene blue (3,7-bis(dimethylamino)-phenothiazin-5-ium chloride, MB), rose bengal (4,5,6,7-tetrachloro-2',4',5',7'-tetraiodofluorescein) and acridine (2,3-benzoquinoline) are known to be efficient $^1O_2$ generators, the vast majority that are successful as PDT agents are based upon the tetrapyrrole chromophore (22). Tetrapyrroles usually have a large absorption band in the region of 400 nm known as the Soret band, and a set of absorption bands as the spectrum gets closer to red wavelengths – known as Q bands (23).

The evaluation of physicochemical properties of a new PS can be performed by spectroscopic techniques and *in vitro* studies can be used to highlight specific applications. Additionally, it is important to screen the absorption, distribution, metabolism and excretion (ADME) properties in order to avoid the clinical failure of drug candidates. According to a survey by Food and Drug Administration (FDA) in 1991, approximately 40 % of clinical failure was due to poor pharmacokinetics (PK) properties (24). Then, pharmaceutical companies began assessing those properties of new chemical entities at the very early stages of drug discovery (25). Several techniques can be used for this screening, such as *in vitro* optimization to understand the specific factors that contribute to the drug disposition, and *in vivo* methods that provide more integrated means for optimizing ADME properties (26).

Starting with the administration, there are three possible routes: enteral route (oral, where the effect is systemic and the substance is given via the digestive tract), parenteral route (the effect is also systemic but the substance is given by routes other than the digestive tract) and topical (the substance is applied directly where its action is desired and the effect is local). Parenteral administration routes include several injections types: intravenous (IV), subcutaneous (SC), intradermal and intramuscular (IM). Many factors affect the drug distribution (*i.e.* its transport from the point of administration or absorption to the site of action), such as the vascular permeability, regional blood flow, cardiac output, perfusion rate of the tissue and the binding ability of the drug to plasma proteins. The lipophilic drug properties that are desirable to its uptake into the biological membranes of its effector site are prejudicial to its elimination of the body. That is why it needs to be metabolized into more hydrophilic metabolites that will be able to pass the renal tubes without being reabsorbed. This metabolic process occurs mainly in the liver, but also in the blood, brain, lung and kidneys. After that, the drug is excreted (renal or biliary; minor: exhalation, sweat) and eliminated from the body (27). **Figure 1.3** resumes the drug route from its administration into the body till its excretion.

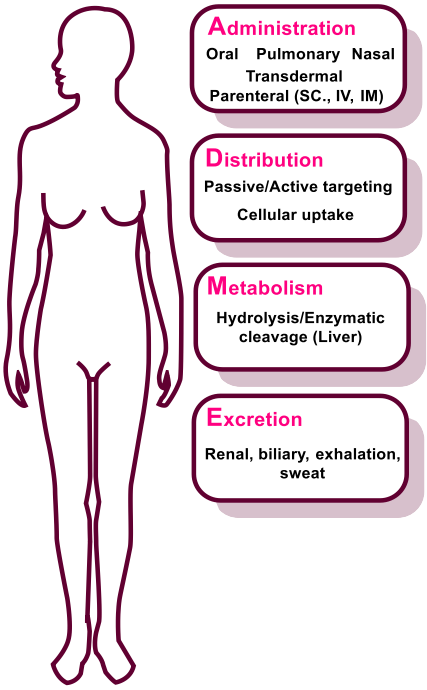

Figure 1.3. Drug ADME route in the human body. Adapted from (28).

First and second generations PSs

The first family of PSs is represented by a purified version of HpD, named Photofrin® (**Figure 1.4**) (29). This was the first PS approved for the treatment of early-stage and advanced lung cancers, superficial gastric cancer, esophageal adenocarcinoma, cervical cancer and bladder cancer (BC), in 1993, in Canada. This PS has an absorption spectrum characteristic of Pors with five peaks (one stronger band – Soret band – and four Q bands). However, Photofrin® is not a pure compound and shows low specificity for the cancer tissue leading to cytotoxic damage in the healthy one like an intense inflammatory and necrotic reaction at the treated site (23). Additionally, it has a low maximum wave absorption band (630 nm), which only allows biological effects at a tissue depth of around 5 mm, after irradiation. Moreover, these sensitizers take 2-3 months to clear from the cutaneous tissues which requires that during this period of time the patients are required to avoid bright light (30).

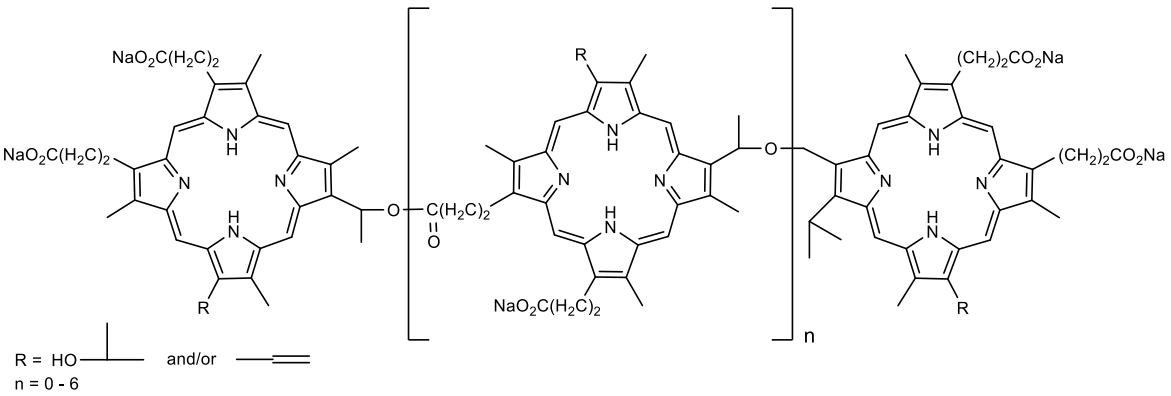

Figure 1.4. Photofrin® structure.

The second generation PSs include, among others, Por derivatives, chlorins and Pcs (*e.g.* Levulan®, Foscan® and silicon(IV) phthalocyanine (Pc4)). They have high ROS production and strong absorption in the required wavelength range (600-850 nm), which allows phototherapy in deep regions, leading to a better efficacy of PDT. Kennedy *et al* demonstrated the clinical suitability of δ-aminolevulinic acid (ALA) (31). Bladder tissue can be photosensitized by instillation of ALA, a prodrug that is able to initiate a series of biochemical reactions that result in significant

accumulation of protoporphyrin IX (PpIX) or photoactive porphyrins (PAPs) that preferentially accumulate in malignant and pre-cancerous tissue rather than in benign cells. However, ALA is an hydrophilic compound and cannot therefore penetrate all tissue, resulting in some clinical limitations, such as a long swelling time and a variable PpIX fluorescence intensity and distribution (32). Chlorins are tetrapyrroles with one pyrrole ring reduced. This feature leads to a higher wavelength absorption band in the region of 650-690 nm which is desirable for PDT (15). Pcs are Por synthetic analogues with excellent photophysical and chemical properties, that together with their chemical versatility, make this class of compounds promising candidates for PDT applications (30). Some of the first and second generation PSs that already are under clinical trial or in clinical use are summarized in **Table 1.1.**

Table 1.1 PSs under clinical trial and in clinical use for malignant diseases.

PS	Chemical class	Name	Indications	Date of approval and country
HpD	Por	Photofrin®	Barrett's esophagus, bladder, lung, cervical, prostate and gastric cancers	1993 in Canada. Now in more than 125 countries
Tetra(m-hydroxyphenyl) chlorin, (mTHPC)	Chlorin	Foscan®	Head, neck, esophageal, gastric and prostate cancers	2001 EU
ALA	Por	Levulan®	Actinic keratoses, hair removal, acne, non-melanoma skin, esophageal and gastrointestinal cancers	1999 in USA and 2000 EU
Hexyl ALA ester	Por	Hexvix®	Diagnosis of bladder tumors	2005 in EU
Lutetiumtexaphyrin	Texaphyrin	Lutex®	Cervical, prostate and brain tumors	Phase II clinical trial
ZnPc	Pc	CGP55847	Squamous cell carcinoma of upper aerodigestive tract	Phase I-III clinical trial
SiPc	Pc	Pc4	Cutaneous/SC lesions from diverse solid tumor origins and sterilization of blood components	Phase I-III clinical trial
Sulfonated AlPc derivatives	Pc	Photosense	Skin, breast, lung and gastrointestinal cancer	Phase I-III clinical trial
F_2BMet	Bacteriochlorin	Luz11	Advanced head and neck cancer	Phase IIa clinical trial

Third generation PSs

The third generation PSs is generated by the coupling of the first or second generation PSs with a targeting component that is specifically recognized by the cancer cell and allows a selective delivery and uptake (30). Pors and their derivatives have been conjugated with many proteins, such as human and bovine serum albumin (HSA and BSA, respectively) (33), monoclonal antibodies (mAbs) (34) and amino acids (35), among others. Alternatively, carbohydrates, that are able to target carbohydrate binding proteins overexpressed in tumoral cells, are also being explored as potential targeting components (36).

In our research group, at the University of Aveiro, several Por glycoconjugates have been developed with very promising results for BC treatment and for antiviral activity against herpes simplex virus type 1 and 2, after PDT (37-40). The glycoconjugates have demonstrated promising *in vitro* results and are currently being tested *in vivo*. Some examples of third generation PSs are represented in **Table 1.2**.

Table 1.2. Third generation PSs and their application.

PS	Biomolecule	Cancer Type
Trastuzumab (34)	mAb-IR700	Breast
Por derivative (33)	HSA BSA	Bladder
Por derivative (35)	Amino acid	Cervical
Por and Pc derivatives (40)	Galacto-dendritic units	Bladder
Chlorin e6 (41)	Maltose	Ovarian Burkitt's Lymphoma
Chlorin derivative (42)	Maltose	Gastric Colon
Por derivative (43)	Galactose Glucose	Liver
Chlorin derivative (44)	Glucose	Gastric Colon
SiPc (45)	Galactose	Liver

4. Phthalocyanines

Pcs have been widely studied due to their potentiality to be used in medicine and supramolecular chemistry (46). In this section their structural and photophysical properties, the synthetic strategies and their role as PS agents will be highlighted.

Structure and properties

Pcs are two-dimensional synthetic tetrapyrrolic compounds constituted by four isoindole units presenting an 18 π-electron system, which is delocalized over an arrangement of alternated carbon and nitrogen atoms. They present a strong absorption band in the red region of the spectrum (630 to 750 nm) mainly in the near-infrared (IR) region (**Figure 1.5**) which confers a bright green/blue color that have a great interest in using Pcs as dyes in pigments industries (47).

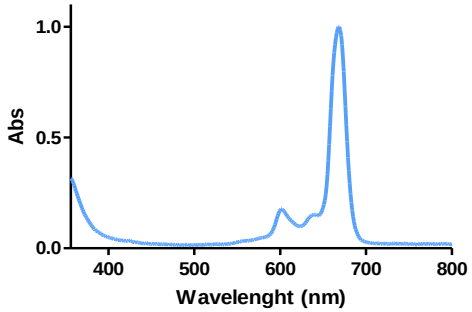

Figure 1.5. Typical UV/Visible (UV/Vis) spectrum of metallo Pcs (MPcs).

These compounds are able to form stable metallocomplexes with many metal cations (*e.g.* zinc (Zn), silicon (Si) and ruthenium (Ru)) using the four central pyrrole nitrogens of the macrocycle (48). The hydrogen atoms of the central cavity can be replaced by more than 70 elements and the coordination number of the square-planar Pc is four. Thus, according to its size and oxidation state, the metal can be inserted into the Pc core. When the metal has a higher coordination number, pyramidal, tetrahedral or octahedral structures result with one or two axial ligands (46). The internal and external positions of the fused benzene ring are also commonly known as α- and β-positions, respectively (**Figure 1.6**). The chemical

versatility of this class of macrocycles allows the tuning of their physicochemical properties, making Pcs promising PS agents for PDT in the treatment of cancer (49).

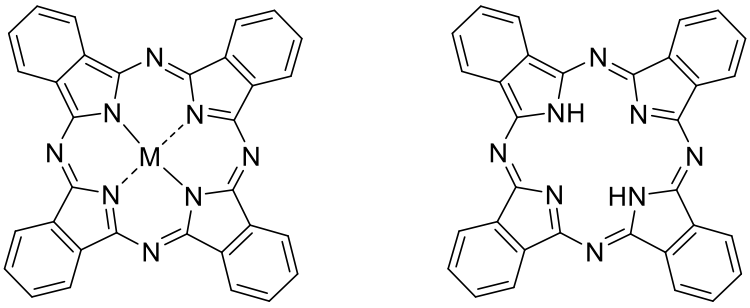

Figure 1.6. Structures of MPc- and metal-free-Pcs (H_2Pc).

Synthetic routes

The synthesis of Pcs can be carried out either by cyclotetramerization of the appropriately substituted precursors, usually phthalonitriles (**Scheme 1.1**) or diiminoisoindolines. Most often, this reaction is conducted in the presence of metal ions that act as template during the ring formation. Not only the metal-template effect, but also the thermodynamic stabilization and the aromaticity involved on the Pc macrocycle formation, are responsible for the ring closure (50).

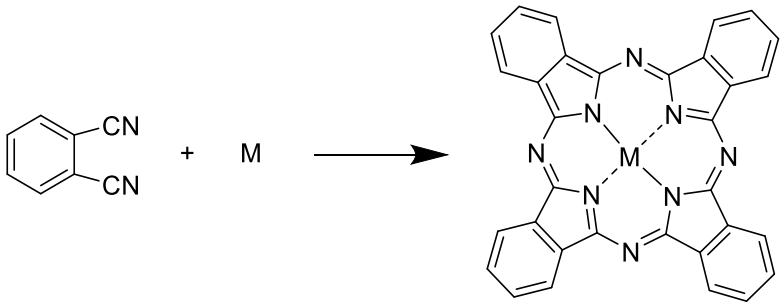

Scheme 1.1. Schematic representation of the synthesis of a MPc using a phthalonitrile as precursor in the presence of metal ions (M).

Owing to their extended conjugation, Pcs exhibit a high aggregation tendency, by π-π interactions and reduction of solubility, that reduce their ADME properties and compromise their photophysical characteristics (i.e. ability to generate $^1O_2$ and other related ROS). To overcome such limitations, a wide variety

of substituents can be introduced either axially or at the periphery of the macrocycle. (47). Due to their promising studies for biological applications, Pcs coordinated centrally with a Si atom will be explored in this dissertation.

4.1 Silicon Phthalocyanines

An important feature of silicon phthalocyanines (SiPcs) is their four-coordinate central atom that allows many structural possibilities and thus a flexibility of the synthetic design, such as the functionalization of two axial ligands (51). The axial functionalization reduces aggregation, increasing the solubility in a variety of solvents, photosensitizing efficiency as well as fine-tune fluorescence and triplet state characteristics (52). The first approved SiPc conjugated with axial ligands was Pc4 (53-55). This PS showed excellent results both *in vitro* and *in vivo* and presently are being made the clinical trials for the treatment of cutaneous neoplasms (56). Pc4 contains two axial ligands consisting of a hydroxyl and a dimethylamino-propylsiloxy group (**Figure 1.7**) and has an absorption band in the therapeutic window (670 nm) (57). This PS demonstrated excellent cellular uptake and photodynamic efficacy as well as effectiveness in eliminating human immunodeficiency virus-infected cells (58).

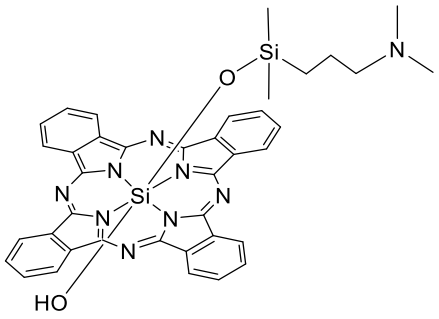

Figure 1.7. Pc4 chemical structure.

Many others axial conjugated SiPcs are being developed and tested *in vitro*, and will be highlighted the ones conjugated with biomolecules, such as proteins (59,60), nucleosides (61), carbohydrates (45, 62-64) and mAb (34) (**Table 1.3**).

Table 1.3. SiPcs axially conjugated to biomolecules and their applications.

Author	Biomolecule	Year, study level	Cancer Type
Huang J. D. (59)	BSA	2003, *in vitro*	Liver
Jiang X. J. (60)	BSA	2006, *in vitro*	Mammary
Shen X. M. (61)	Nucleosides	2013, *in vitro*	Liver
Lau J. T. F. (62)	β-cyclodextrin	2011, *in vitro*	Colorectal
Lo P. C. (63)	Acetal-protected glucose	2007, *in vitro*	Colorectal
Lee P. P. S. (45) Lo P. C. (64)	Acetal-protected galactose	2005, *in vitro* 2007, *in vitro*	Liver Colon
Mitsunaga M. (34)	mAb	2010, *in vivo*	Epidermoid

4.2 Phthalocyanines galacto-dendritic conjugates

Pc's tendency of aggregation due to their low solubility in many solvent systems is being a challenge in the development of effective Pc formulations. Aggregation of the macrocycle leads to quenching of the ^{3}PS*, decreasing the yield of triplet state and hence the efficiency of the compound as a PS (46). In order to minimize these problems, the development of new Pcs linked to biochemical motifs have been developed.

Carbohydrates are potential candidates as PS-delivery systems because they are biocompatible molecules with a rapid cellular uptake and with a specific recognition by lectin proteins (36). Lectins' hydroxyl groups make the sugars suited for directional acceptor/donor hydrogen bonds (65). It is expected that the specific (non-covalent) binding of carbohydrates with lectins promotes the accumulation of the glycoconjugate inside cells by the endocytic pathway (66). Furthermore, certain carbohydrate-binding lectins are overexpressed in tumor cells (67). Therefore, galactose molecules have been conjugated with PSs, since they can be recognized by galactose-binding proteins overexpressed in cancer cells (namely galectin-1 and -3) (68). Galectins are small soluble proteins (molecular weight 14-35 kDa) with carbohydrate recognition domains (CRDs) which are responsible for the specific and individual binding of each galectin to carbohydrates (69). Particularizing to galectin-

1, this protein exhibits dual localization, being found in both intracellular (nucleus and cytoplasm) and extracellular (cell surface and medium) compartments (70). Intracellularly, it is involved in fundamental processes such as pre-mRNA (precursor messenger ribonucleic acid) splicing and on the regulation of intracellular signaling pathways (*e.g.* mitosis, apoptosis and cell-cycle progression) after binding intracellular ligands. Extracellularly, it can bind to cell-surface glycoconjugates that contain suitable galactose-containing oligosaccharides (71). Therefore, the coupling of a Pc with galactose moieties can provide a distinct advantage for the efficacious targeting of the PS to cancer cells due to the presence of galactose-binding proteins that are overexpressed in those cells, and that can facilitate the PS cellular uptake (**Figure 1.8**).

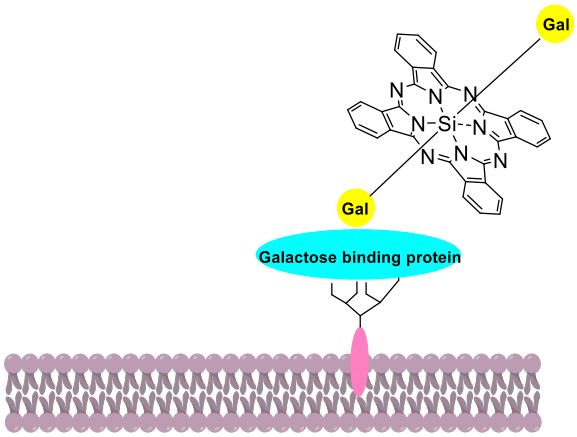

Figure 1.8. Possible interaction of a SiPc conjugated with two galactose molecules with galactose binding proteins overexpressed in cancer cells.

Many PSs conjugated with carbohydrates showed promising *in vitro* results and are currently being tested *in vivo*. Maillard reported the synthesis of a glycoconjugated chlorin (42). Fujimoto has conjugated a Por with galactose and its molecular delivery to hepatocytes (43). Silva reported the synthesis of a Pc containing eight dendritic units of galactose (72) which is able to target and kill BC cells through mediated interaction with galactose-binding proteins overexpressed in those cells (40). Particularizing to SiPcs, there are only few reports of their axial conjugation to carbohydrates. Ng and co-workers reported the conjugation of unsymmetrical SiPcs with a β-cyclodextrin (62), of two SiPcs with acetal-protected glucose molecules (63) and also a SiPc with one or two axial acetal-protected

galactose substituent(s) (**Table 1.3**) (45). The *in vitro* and *in vivo* results showed a high photodynamic activity of these compounds against HepG2 human hepatocellular carcinoma, which can be attributed to the high cellular uptake and efficiency to generate $^1O_2$, as well as tumor growth retardation. These compounds are therefore promising PSs for PDT. However, there are no reports related with the synthesis and validation of SiPcs conjugation with deprotected sugar substituents.

Recently, the emerging role of dendrimers in biological systems has highlighted their potential benefits for the preparation of new anticancer drugs. Dendrimers are highly branched nanostructures with many arms emanating from a central core (73). Besides improving the biocompatibility and the photochemical proprieties of PSs, they also create multivalent interactions with more than one receptor binding site, contributing to an active cancer cell targeting, improving cellular recognition (**Figure 1.9**). Additionally, they act as nanocarriers, leading to the enhanced permeability and retention (EPR) effect that is characteristic of tumor tissues (37). Several PSs (Por and Pc) conjugated with galacto-dendritic units have been synthesized and tested *in vitro* in BC cells with very promising results (40,72). However, there are no reports of the axial conjugation of Pcs with galacto-dendritic units.

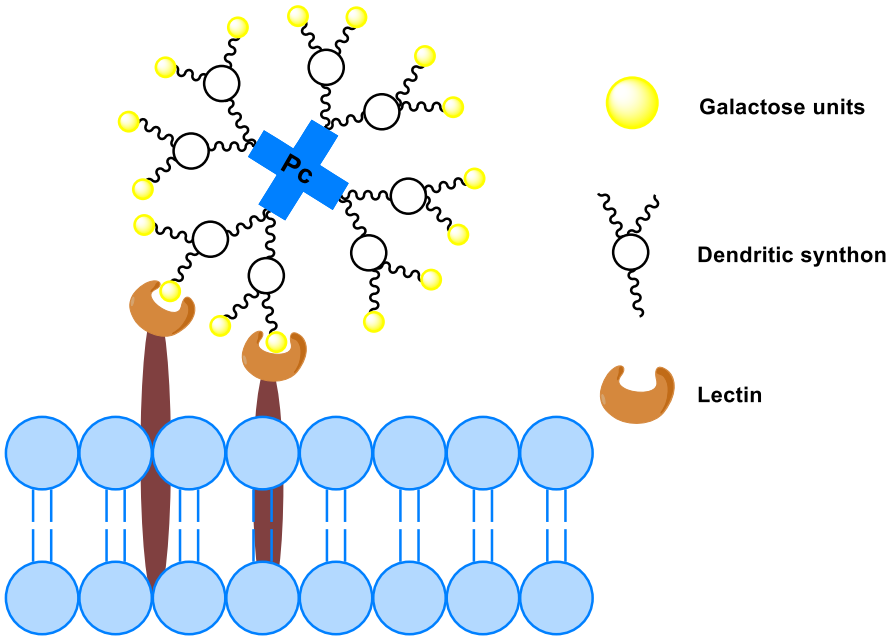

Figure 1.9. Illustration of the interaction of a Pc conjugated with eight galacto-dendritic units to a lectin overexpressed in tumoral cells. Adapted from (40).

5. Photodynamic therapy in clinical applications

PDT has been mostly restricted to the treatment of melanomas and solid tumors occurring in externally accessible cavities, like the bladder and the esophagus (3). PS can be administrated intravenously or topically and then it should be preferentially accumulated in the desired tissue (**Figure 1.10**). After a predetermined time, known as the drug-to-light interval, light is directly applied into the tumor by the use of modern fiber-optic systems and various types of endoscopy, which allows an accurately light targeting to almost any part of the body (74). The period of time between PS administration and the start of illumination varies between 5 min to 24 h, or more. The most efficient light systems are lasers and light emitting diodes (LEDs) sources with relatively narrow spectral bandwidths and high fluence rates. Lasers can also be coupled into fibers with diffusing tips to treat tumors in the urinary bladder and the digestive tract (3).

$^1O_2$ generated by the activated PS is believed to be responsible for tumor destruction (75). Once $^1O_2$ has a very short lifetime, it is deactivated before it can escape from the cell in which it was produced. Photobleaching can be an advantage avoiding an overall skin photosensitivity which is one of the main side effects in patients treated with PDT. Total healing of the area after PDT may take from 2 to 6 weeks. During this time, the patient will be light sensitive (due to PS accumulation in the skin) and must be protected from direct light (3).

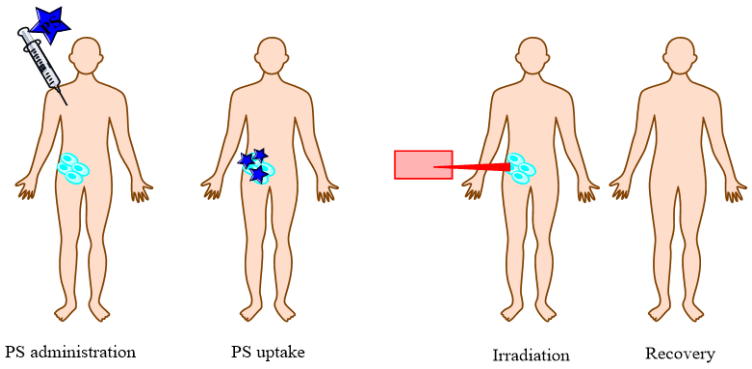

Figure 1.10. PDT protocol in oncology. Adapted from (76).

In order to improve the therapeutic index of treatments in modern oncology, many therapeutic modalities with non-overlapping toxicities can be combined. There are two general approaches that may increase the antitumor effectiveness of PDT, mostly in elderly or debilitated patients who less tolerate more intensive therapeutic regimes, such as: i) sensitization of tumor cells to PDT (77) and ii) interference with cytoprotective molecular responses triggered by PDT in surviving tumor or stromal cells. Therefore, any interactions between PDT and PSs will be confined to the irradiated area (3). Despite all its applications, PDT has the limitation that cannot cure advanced disseminated diseases because it requires irradiation of the whole body with appropriate doses and that is not possible with the present technologies. However, for advanced diseases, PDT can improve quality of life and lengthen survival of the patients (74). For early or localized diseases, this technique can be a selective and curative therapy with many potential advantages over available alternatives.

5.1 Bladder Cancer

BC is a disease that affects many patients worldwide. It has a high rate of mortality and recurrence (78). Nowadays, many advances have been attempted to understand the nature of this disease and to develop new treatment approaches (79). In this section, the focus is on BC physiopathology, incidence and treatment.

Physiopathology

Bladder is a hollow, balloon shaped organ in the pelvic floor containing three histological layers: 1) urothelium, 2) lamina propria (suburothelial loose connective tissue) and 3) detrusor or muscularis propria. After muscularis propria there is a perivesical fat that covers the superior surface and the upper part separating the bladder from the nearby organs (**Figure 1.11**) (80,81). Urothelium is a highly specialized transitional epithelium layer that creates an interface between pathogens and other bladder tissues through many defense mechanisms. Its cell

turnover is very slow, but capable of a very rapid proliferation in response to injury (82).

BC progression is based on four stages that depend on the location of the tumor in the bladder layers. The tumor grows from the inside of the bladder wall (stage 0) and can spread into the lamina propria layer (stage I), then into the muscular layer (stage II), penetrate the perivesical tissues (stage III) and finally invade other organs (stage IV): prostate, uterus, vagina, abdominal wall and pelvic wall (**Figure 1.11**). Stages 0 and I are superficial or non muscle-invasive while stages II, III and IV are muscle-invasive cancers. When the cancer extends from its original place (in the bladder) to another part of the body (stage IV) it is named metastatic BC (79). The classification of BC staging comes from the Tumor-Node-Metastases (TNM) system which is based on the size and penetration of the tumor on the tissues of the bladder (**Table 1.4**) (81).

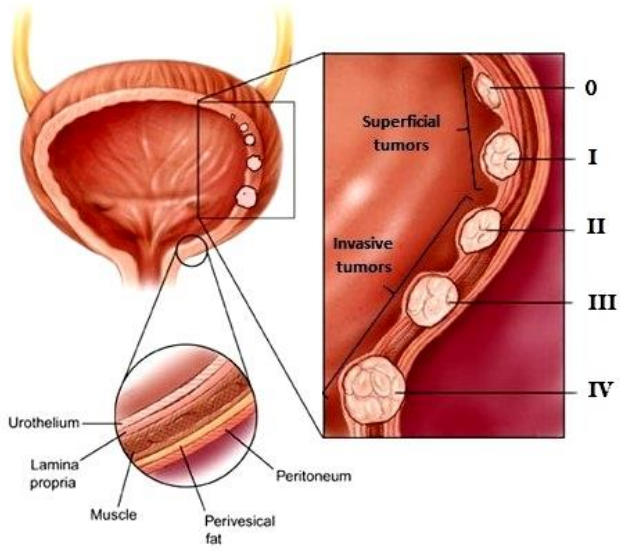

Figure 1.11. Bladder layers and BC progression. Adapted from (83).

Table 1.4. Staging of primary BC tumors (TNM classification) (81).

Primary tumor (T)	
T0	No evidence of primary tumor
Ta	Noninvasive papillary carcinoma
Tis	Carcinoma *in situ* (CIS): "flat tumor"
T1	Tumor invades lamina própria
T2	Tumor invades muscularis propria
T2a	Tumor invades superficial muscularis propria (inner half)
T2b	Tumor invades superficial muscularis propria (outer half)
T3	Tumor invades perivesical fat
T3a	Tumor invades perivesical fat microscopically
T3b	Tumor invades perivesical fat macroscopically
T4	Tumor invades prostate, uterus, vagina, pelvic wall and abdominal wall
T4a	Tumor invades prostate, uterus and vagina
T4b	Tumor invades pelvic wall and abdominal wall

The staging process is a major factor in treatment choice. BC is a pathology that frequently does not have symptoms associated. However, when it does, the most common ones are painless hematuria, that can be detected by a chemical reagent strip for hemoglobin and spun sediment microscopy on voided urine, and irritative symptoms such as frequency, urgency and pain. Normally, screening is performed by combining different modalities: the surgical procedure transurethral resection (TUR), bimanual palpation before and after TUR, fluorescence cystoscopy, radiological imaging techniques and histopathological examination (79).

The non muscle-invasive BC (Ta (70%) and T1 (20%), **Table 1.4**) is the most frequently diagnosed. Its progression to muscle-invasive BC and rate of recurrence depends on the tumor grade, stage and size, the presence of CIS (**Table 1.4**), the occurrence of multifocal lesions and the prior recurrence. Ta tumors rarely become muscle-invasive, but high grade T1 tumors and flat CIS lesions (**Table 1.4**) have an increased propensity to progress. Although CIS belongs to the non muscle-invasive

(10%) BC group, it is associated to a higher aggressiveness due to molecular alterations that are characteristic of muscle-invasive BC (84).

Statistics

BC is the 9th most common cancer worldwide. The age standardized rate (ASR) is 10.1 per 100,000 for males and 2.5 per 100,000 for females. More than 12 million of new cancer cases occur annually worldwide, of those 5.4 million occur in developed countries and 6.7 million in developing countries (78). In Europe, mortality rates increased in Southern and Eastern Europe between the mid-1950s and late 1980s, but a decline has been observed in several Northern European countries over the last two decades (79).

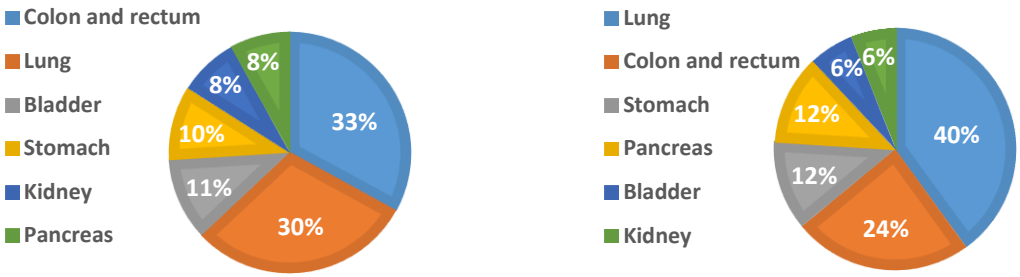

Figure 1.12. Most frequent cancers in Europe (2012). The values correspond to estimated incidence (left) and mortality (right) in both males and females (85).

Predisposition factors include smoking, exposure to aromatic amines and inorganic chemicals in the workplace, chronic cystitis associated with foreign bodies, pelvic radiation therapy, exposure to the chemotherapeutic prodrug cyclophosphamide (79) and parasitic infections (86) in the Middle East and parts of Africa where schistosomiasis is a widespread problem. Most bladder carcinogens exert their action by direct contact with the bladder epithelium. Inhaled or ingested compounds that are either directly carcinogenic or that can be transformed by the body in carcinogenic byproducts, reach the urinary bladder because they are excreted via the urine. Patients that had BC histories for recurrence need to be

screened annually by cytological examination of exfoliated cells in both voided urine and saline bladder lavage specimens (79).

Treatment

BC treatment depends on the grade, stage and whether the lesion is flat or papillary (87). The most applied surgical procedure is TUR that can be used to diagnose, stage, and treat the majority of primary and recurrent bladder tumors. This treatment has three main goals: i) to provide pathologic material to determine the histologic type and grade of bladder tumor; ii) to determine the presence, depth and type of tumor invasion; and iii) to remove all visible and microscopic superficial and invasive tumor(s) (88). If there are multiple recurrences, the patient is given a topical immunotherapy that consists in intravesical instillations of Bacillus Calmette-Guerin (BCG). This therapy is only applied in non muscle-invasive BC with no side effects and is an easy deliver in bladder due to its great accessibility (89). However, this treatment fails in 30-40% of patients, and 30-40% of those had an initial response that relapsed due to intolerance, recurrence and resistance of patients to BCG (90). In more advanced stages of the tumor, radiotherapy, radical cystectomy and chemotherapy are the therapeutics of choice (91,92). Though, these conventional therapies might cause unwanted side effects and in some cases they are not completely effective in the destruction of the tumor, leading to a high risk of recurrence and progression. Thus, in order to preserve the bladder and its function, there is a clinical interest on using alternative treatments.

The clinical urological interest in PDT is focused on the preservation of the organ and its function because there are no significant changes in tissue temperature, and the preservation of connective tissue leads to minimal fibrosis. Current scientific research on PDT for BC treatment is based on the development of tumor selective drugs (33, 40, 93). BCs are suitable targets for PDT because their interior can be assessed by endoscopy. The bladder geometry should allow an improved and homogeneous light delivery and the bladder tissue is relatively more translucent when compared to other human tissues (3). The first PS used to treat recurrent BC was HpD, in 1975 (94). After this, in 1993, Photofrin® was approved in

Canada. However, both PSs could only be used for superficial BC, once for whole-bladder PDT, there was a high incidence of side effects, such as urinary frequency, pain and persistent reduction in bladder capacity (23, 95, 96). These complications were due to the excessive light doses and the non-uniform light delivery in the early studies. Nseyo *et al* showed that, for standardized protocols, reducing the drug and light dose and decreasing the light penetration in tissues to wavelengths of 514 nm (green light), also gives a good tumor response rate for superficial lesions without transmural bladder wall injury or treatment-related morbidity (97). This became an excellent treatment option of CIS, although it was not been fully evaluated. Another PS that has been used for recurrent superficial bladder cancer is Levulan® by given a single PDT treatment or in combination with mitomycin C, which resulted in a complete response rates at 18-24 months without persistent reduction in bladder capacity (98-101). Finally, as mentioned before, various therapeutic modalities with non-overlapping toxicities could also be combined. Pan *et al* (102) hypothesized that PDT combined with intravesical BCG would form an auto-vaccine for BC. Tumor cells treated *in vitro* by PDT can be used to generate potent cancer vaccines. Hypothetically, tumor cells destroyed by PDT could be treated with BCG to elicit and amplify the immunological response, which would lead to the formation of an *in-situ* auto-vaccine against urothelial tumor cells, whether local or systemic.

6. Objectives and working plan

The necessity of finding new approaches for cancer treatment in order to preserve the quality of life of the patient by reducing side effects has been captivating the attention of many research groups. Being PDT a less invasive therapy that selectively attack the cancer cells, the goal is to find ideal PSs suitable for many types of cancers. BC is a good target for PDT due to its geometry that allows an endoscopy access.

An ideal PS is not always easy to find because it should be endowed with specific features as described above (page 7). The development of Pcs for PDT has been especially promising due to their unique photochemical properties. However, Pcs have reduced water solubility and low specificity to the cancer tissue. Therefore, the aims of this Master's dissertation were to synthesize water soluble SiPcs conjugated with galacto-dendritic units that will increase the specificity to tumoral cells, to study their photophysical and photochemical properties, and to validate them as photodynamic therapeutic agent against BC cells.

Working Plan

- Synthesis of novel water soluble galacto-conjugated SiPcs;
- Study of their photophysical and photochemical properties:
    - Solubility in DMSO, DMF (Dimethylformamide) and PBS (Phosphate buffered saline);
    - Fluorescence emission spectrum in DMF;
    - Photostability when irradiated with red light;
    - Generation of $^1O_2$ using DPBF as $^1O_2$ scavenger;
- Validate their photodynamic potential against a human bladder cancer cell line, UM-UC-3, with high levels of galectin-1:
    - Determine the uptake of the galacto-conjugates by BC;
    - Quantify the levels of ROS after PSs-PDT;
    - Determine the toxicity in darkness (MTT assay);
    - Determine the phototoxicity after light activation (MTT assay);

The elaboration of this master thesis took place in three different institutions under the supervision of Dr João Tomé (University of Aveiro, UA), Dr Tomás Torres Cebada (University Autonoma of Madrid, UAM) and Dr Rosa Fernandes (Institute for Biomedical Imaging and Life Sciences, IBILI, from Medical Faculty of Coimbra). At UAM and UA was performed the synthesis of the PSs, at UA the photophysical and photochemical studies and at IBILI the photobiological studies.

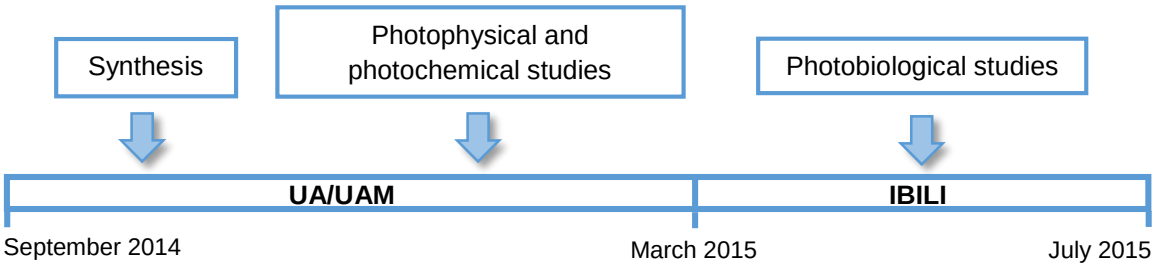

Scheme 1.2 Chronology and institutions involved in the studies of this thesis.

CHAPTER II

RESULTS AND DISCUSSION

Part 1.
Novel galacto-conjugated silicon phthalocyanines: synthesis and characterization

1. Novel galacto-conjugated silicon phthalocyanines: synthesis and characterization

1.1 Overview

Nowadays, PDT research is focused on the development of new PSs with improved photophysical and photobiological properties (3). Pcs derivatives have high absorption in the visible region of the spectrum (around 650 nm), allowing much deeper tissue penetration for therapy. These PSs present a long lifetime of the triplet excited state which will induce high production of $^1O_2$ (49). Based on these properties, Pcs have emerged as a promising class of PSs (103). However, the major problem is their insolubility in physiological fluids due to their hydrophobic skeletons, which leads to Pcs aggregation, affecting their photophysical properties. Additionally, the Pcs' core has not specificity for cancer cells. To overcome that, a wide variety of substituents can be introduced either axially or at the periphery of the macrocycle (40, 45, 93). Knowing that cancer cells have increased levels of galactose-binding proteins, the combination of carbohydrate moieties with macrocycles improves PS uptake and PDT efficacy. Furthermore, these carbohydrate units can also provide water-solubility to the macrocycles (16).

The aim of this section is to describe the synthetic steps attempted to obtain SiPcs conjugated axially with galacto-dendritic units (**Figure 2.1**). The structure of the compounds was corroborated using spectroscopic and spectrometric techniques (nuclear magnetic resonance NMR, matrix-assisted laser desorption/ionization MALDI-MS and electrospray ionization mass spectrometry, ESI^+-MS). These studies were performed at University Autonoma of Madrid and University of Aveiro.

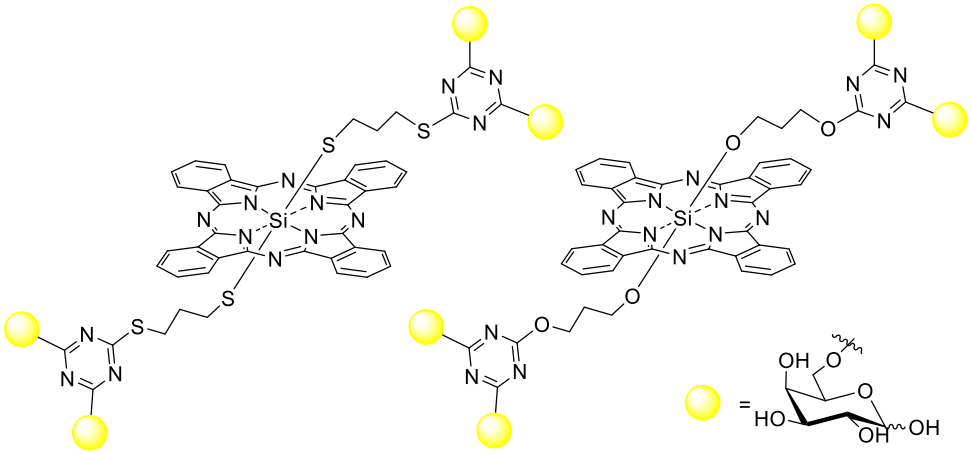

Figure 2.1 SiPcs axially conjugated with two galacto-dendritic units.

1.2 Synthesis of galacto-dendritic units

Herein we report the synthesis of two galacto-dendritic units, differing only in the linker chain, and their further axial coordination with the SiPc macrocycle (**Scheme 2.1**). 1,2:3,4-di-*O*-isopropylidene-α-D-galactopyranose was chosen as the carbohydrate moiety, in order to relate these new compounds with our previous studies, which have already shown the importance of this carbohydrate unit in the photophysical, photochemical and photobiological results (15, 40, 72, 104). The selected dendritic framework was 2,4,6-trichloro-1,3,5-triazine (TCT) because of its well-known selective reactivity concerning the substitution of each chlorine atoms at different temperatures. The synthesis of dendritic units **2** and **3** was performed in two steps as depicted in **Scheme 2.1**. Although dendritic unit **3** is less nucleophilic than dendritic unit **2**, it was expected that the electronegativity of the oxygen atom would allow the formation of a more stable bond with the silicon atom of the SiPc core than the one formed with the sulfur atom (105).

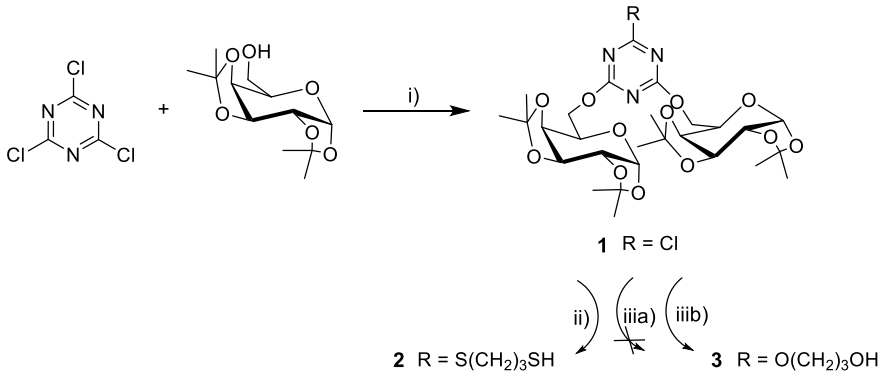

Scheme 2.1. Synthetic route for the preparation of galacto-dendritic unit **2** and **3**. i) DIPEA, toluene, Ar, 60 ºC, 66%; ii) DIPEA, toluene, Ar, 70 ºC, 75%; iiia) NaH, toluene, Ar, 70 ºC, 89%; iiib) DIPEA, toluene, 80 ºC, 61%.

Compounds 2-chloro-4,6-bis(1,2:3,4-di-*O*-isopropylidene-α-D-galactopyran-6-yl)-1,3,5-triazine [**1**] and 3-[(4,6-bis(1,2:3,4-di-O-isopropylidene-α-D-galactopyran-6-yl)-1,3,5-triazin-2-yl)thio]propane-1-thiol [**2**], were prepared according to a literature procedure, as shown in **Scheme 2.1** (72). The nucleophilic substitution of the TCT by the galactose moieties was carried out in dry toluene, in the presence of an excess of *N,N*-diisopropylethylamine (DIPEA) and stirred during 48 h, under argon (Ar). The desired compound was purified by column chromatography on silica gel using a mixture of hexane (Hex) and ethyl acetate (AcOEt) (8:2 to 7:3 v/v) as eluent with a 66% of yield (lower than the one reported in the literature) (72). The carbohydrate units are linked to the TCT by the hydroxyl group located in carbon C-6. The following step to produce compound **2**, was based on the addition of 1,3-dimercaptopropane to compound **1** in a reaction mixture with the same conditions as the ones to achieve compound **1**, providing compound **2**, with an yield of 75% (lower than the one reported in the literature) (72).

To obtain the new compound **3**, 1,3-dipropanediol was added to compound **1**, in a reaction mixture by using the same conditions employed for the synthesis of compound **2**, but using sodium hydride (NaH) instead of DIPEA. The NMR and ESI^+ MS studies demonstrated that the desired compound was not obtained because NaH hydrolyzed the galactose moieties of compound **1**. Therefore, NaH was substituted by DIPEA, and compound **3** was obtained with 61% yield.

The ^{1}H NMR spectrum of compound **1** showed four singlets between δ 1.31-1.49 ppm attributed to the isopropylidene methyl groups. The proton 5'-H appeared as a triple doublet at δ 4.18 ppm (*J* = 1.4, 6.4 and 6.5 Hz). The signals of protons 4'-H and 2'-H emerged as multiplets at δ 4.31 ppm, while the protons 6'-H came out at δ 4.53 ppm. The signal of the proton 3'-H appeared as a double doublet at δ 4.62 ppm (*J* = 2.4 and 7.9 Hz). Finally, the doublet at δ 5.52 ppm (*J* = 5.0 Hz) was attributed to the resonance of the 1'-H.

Regarding compound **2**, the ^{1}H NMR spectrum also showed four singlets between δ 1.32-1.49 ppm attributed to the resonances of the isopropylidene methyl groups. Then the 1,3-dimercaptopropane methylene and thiol groups appeared as multiplet signals: H_b ($CH_2\underline{CH_2}CH_2SH$) δ 2.02, H_c ($CH_2CH_2\underline{CH_2}SH$) 2.64, 2.75-2.80 (SH) and H_a ($\underline{CH_2}CH_2CH_2SH$) 3.23 ppm. The remaining signals of the galactoses' protons were the same as the ones corresponding to compound **1**.

Finally, compound **3** had a ^{1}H NMR spectrum, shown in **Figure 2.2**, similar of compounds **1** and **2,** having also two multiplets and a double doublet corresponding now to the 1,3-propanediol methylene groups: H_b ($CH_2\underline{CH_2}CH_2OH$) δ 1.99, H_c ($CH_2CH_2\underline{CH_2}OH$) 3.76 and H_a ($\underline{CH_2}CH_2CH_2OH$) 4.54 ppm (*J* = 6.3 Hz), respectively. These last three signals were not observed in the ^{1}H NMR spectrum of the final product prepared when using NaH as a base (route iiia), **Scheme 2.1**), which was the proof that we did not obtained the desired compound. The structure of the galacto-dendritic unit **3** was confirmed by mass spectrometry.

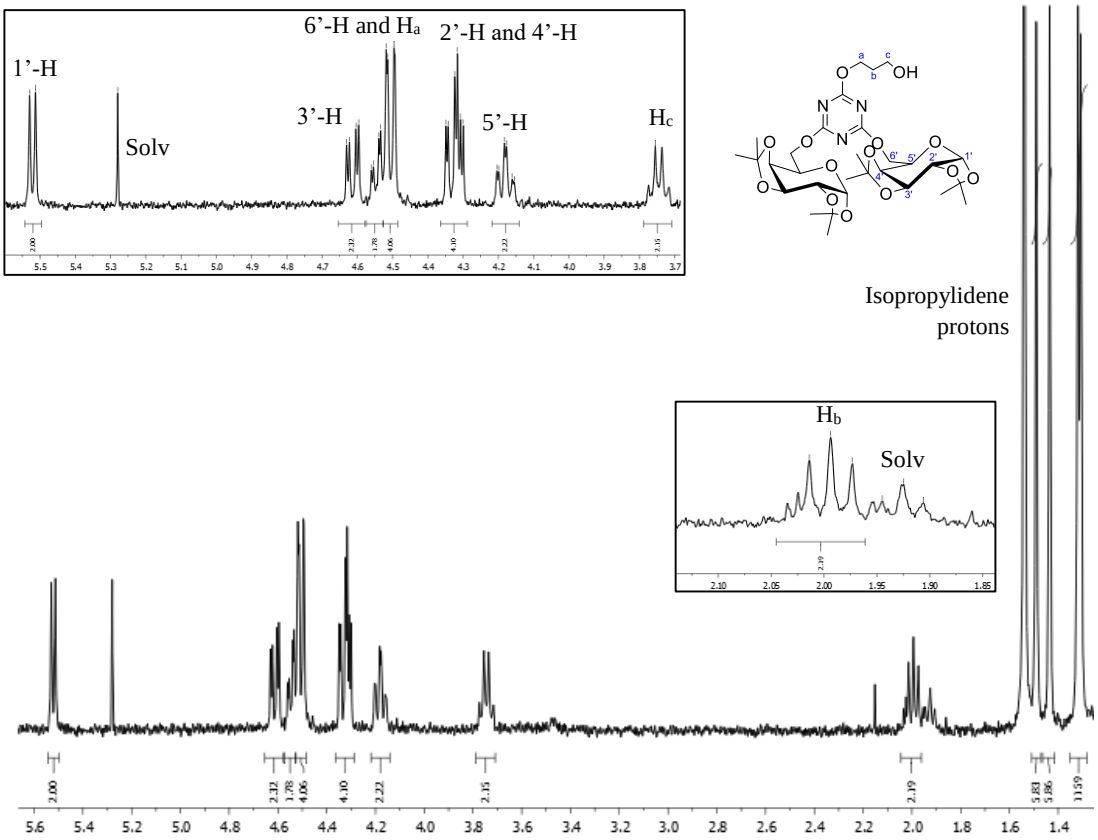

Figure 2.2. ^{1}H NMR spectrum of galacto-dendritic unit **3** in $CDCl_3$ solvent. Inset: expansions of the ^{1}H NMR spectrum.

1.3 Synthesis of galacto-conjugated silicon phthalocyanines

1.3.1 Synthesis of a symmetrical silicon phthalocyanine axial conjugated with galactose moieties [**4**]

The synthetic route to achieve SiPc **4** (**SiPcGal$_2$**, *i.e.* a SiPc containing two monomers of acetal-protected galactose) depicted in **Scheme 2.2,** it is already described in literature (45) and was prepared for comparative purposes with the SiPc conjugated axially with the aforementioned galacto-dendritic units **2** and **3**. The commercially available silicon(IV) phthalocyanine dichloride ($SiPcCl_2$) was treated with 1,2:3,4-di-*O*-isopropylidene-α-D-galactopyranose in the presence of NaH, in toluene reflux, under argon (Ar), during 48 h, giving the di-substituted SiPc **4** in 53% yield (higher than the one reported in the literature) (45). This compound was highly

soluble in a wide range of organic solvents and could be purified readily by column chromatography on silica gel. Then, once the aim of this newly PSs was to be recognized by the galactose-binding proteins overexpressed in cancer cells, it was necessary to hydrolyze the isopropylidene groups of the galactose molecules. The hydrolysis attempts were performed by employing two different approaches: i) by using TFA/H_2O (9:1) as solvent, at room temperature (rt), during 5 h (72); and ii) with bromotrimethylsilane (TMSBr), using dichloromethane (DCM) as solvent, at rt, during 24 h (106). However, both hydrolysis resulted in the loss of the galactose molecules, thus producing SiPc dihydroxide (**SiPc(OH)$_2$**).

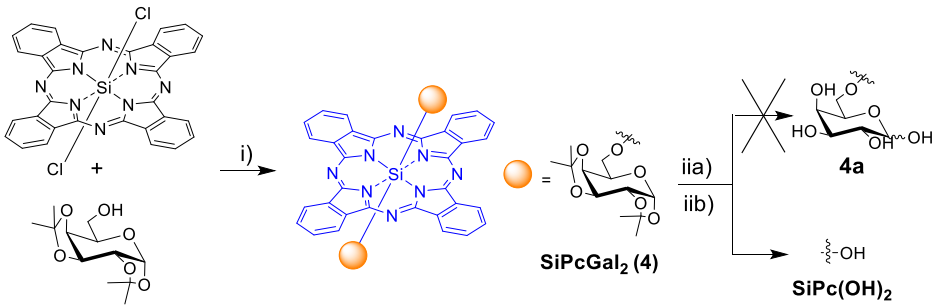

Scheme 2.2. Synthetic route for the preparation of SiPcs **4** and **SiPc(OH)$_2$** i) NaH, toluene reflux, Ar, 53%; iia) TFA/H_2O (9:1), rt; iib) TMSBr, DCM, rt.

The ^{1}H NMR spectrum of SiPc **4** was well-defined. Upfield there were two double doublets that corresponded to the 6'-H protons: δ -2.37 (*J* = 8.8 and 9.3 Hz) and -1.70 (*J* = 5.3 and 8.3 Hz) ppm. The protons of the isopropylidene methyl groups appeared as singlets between δ 0.30 and 0.79 ppm. In the middle of this range, it was also possible to observe protons 5'-H at δ 0.68 ppm, which emerged together, in a virtual singlet, with one of the isopropylidene methyl groups. Proton 4'-H was localized at δ 0.76 ppm as a double doublet (*J* = 0.8 and 9.2 Hz). Then, there were two double doublets, 3'-H and 2'-H, at δ 3.22 (*J* = 0.4 and 8.5 Hz) and 3.32 (*J* = 1.6 and 5.4 Hz) ppm, respectively, and a doublet corresponding to 1'-H at δ 4.37 ppm (J = 5.0 Hz). Finally, downfield there were two multiplets corresponding to the SiPc macrocycle: Pc-H_α protons appeared between δ 8.28 and 8.31 ppm and then the

Pc-Hβ since δ 9.59 to 9.62 ppm. Through mass spectroscopy the structure of the SiPc **4** was confirmed.

1.3.2 Synthesis of a symmetrical silicon phthalocyanine axially conjugated with compound **2** [**5**]

In order to obtain SiPc **5**, $SiPcCl_2$ was treated with compound **2** in DMF and the reaction was refluxed under Ar, during 24 h (**Scheme 2.3**). This condition was optimized according to a procedure described in the literature (107). Yet, the desired compound was not obtained, indeed the 1,2:3,4-di-O-isopropylidene-a-D-galactopyranose signals were not observed in the corresponding ^{1}H NMR spectrum.

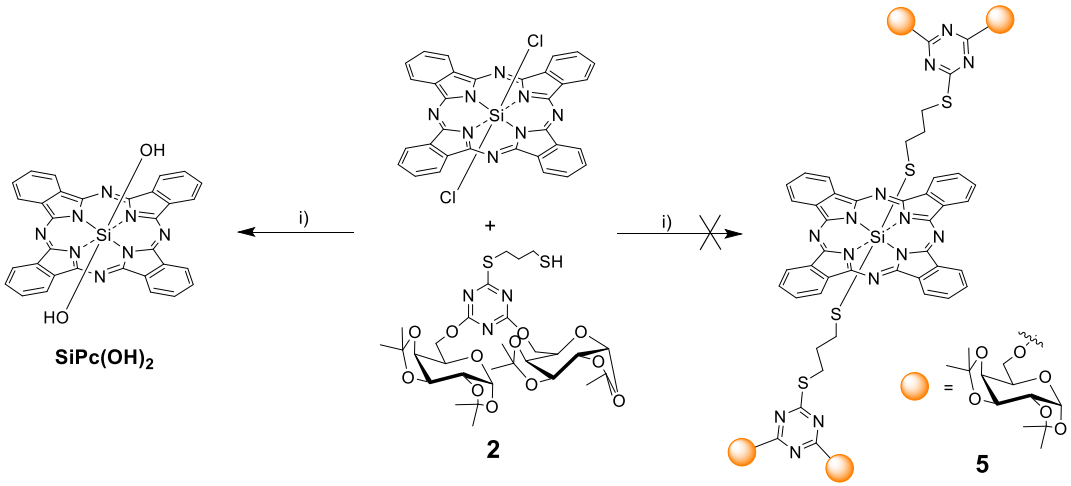

Scheme 2.3. Synthetic route for the preparation of SiPc **5.** i) DMF, Ar, reflux.

1.3.3 Synthesis of a symmetrical silicon phthalocyanine axially conjugated with compound **3** [**6**]

The SiPc **6** was prepared by a reaction between the $SiPcCl_2$ and five equivalents of **3** in the presence of pyridine as base and in toluene. The reaction was allowed to reflux for 72 h, giving the di-substituted SiPc **6** in 61% yield. This conditions were optimized according to the work of Ng *et al*, who described the axial coordination of a SiPc with 3- or 4-hydroxypyridine (108). SiPc **6** was highly soluble

in a wide range of organic solvents and could be easily purified by column chromatography on silica gel. Then, as last step, the hydrolysis of the isopropylidene protective groups was performed by using the same methodology employed for the preparation of SiPc **4** (**Scheme 2.4**), but unfortunately, once again, we obtained the dihydroxy derivative **SiPc(OH)$_2$**.

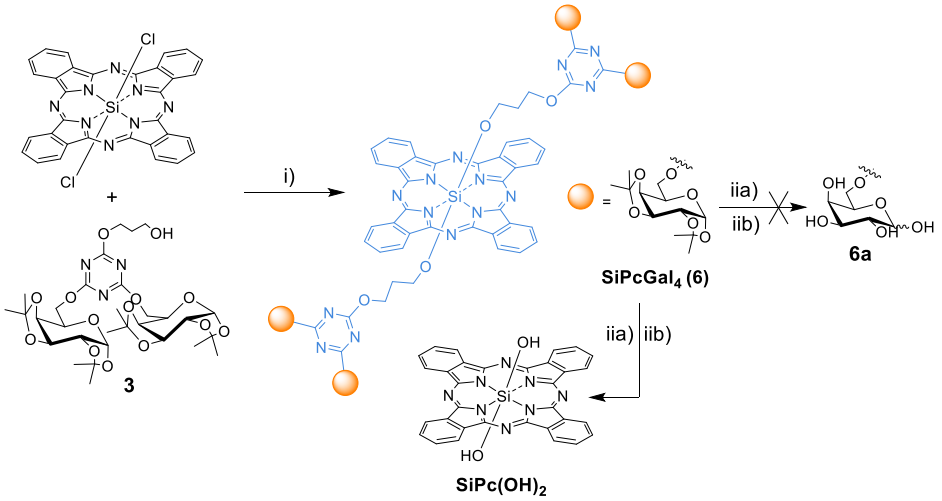

Scheme 2.4. Synthetic route for the preparation of SiPcs **6** and **SiPc(OH)$_2$.** i) Pyridine, toluene reflux, Ar, 12%; iia) TFA/H_2O (9:1), rt; iib) TMSBr, DCM, rt.

The ^{1}H NMR spectrum of SiPc **6** was well-defined (**Figure 2.3**). Upfield there were two triplets (H_c and H_a) and one multiplet (H_b) that emerged at: δ -1.99 (*J* = 6.5 Hz) and 0.00 (*J* = 3.9 Hz) for the triplets and -1.06 ppm for the multiplet. The resonances of the isopropylidene methyl groups appeared as singlets between δ 1.38 and 1.55 ppm. Protons 5'-H exhibited a triple doublet at δ 4.22 ppm (*J* = 1.0, 4.0 and 4.0 Hz), protons 4'-H, 2'-H and 6'-H emerged as multiplets at δ 4.32, 4.39 and 4.42 ppm, 3-H' protons resonance came out as a double doublet at δ 4.69 ppm (*J* = 4.7 and 1.4 Hz) and the doublet at δ 5.64 ppm (*J*= 2.9 Hz) corresponded to 1'-H. Downfield there were two multiplets corresponding to the Pc-protons: first the Pc-H_α protons between δ 8.29 and 8.31 ppm and then the Pc-H_β since δ 9.55 to 9.57 ppm. Through mass spectroscopy the structure of the SiPc **6** was confirmed.

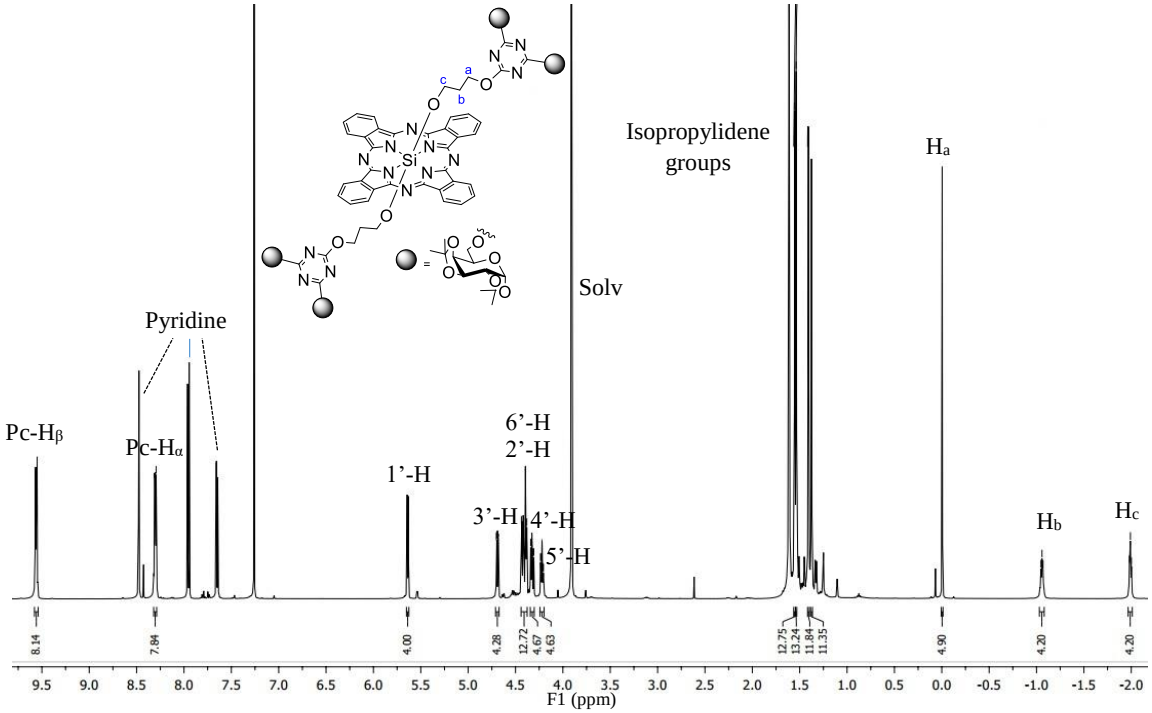

Figure 2.3. ^{1}H NMR spectrum of SiPc **6** in $CDCl_3$ solvent.

Regarding all these reactions and final products obtained, the studies performed in this thesis (photochemical, photophysical and photobiological studies) were carried out using SiPcs **4** and **6**, which were named as **SiPcGal$_2$** and **SiPcGal$_4$**, respectively. Even though some photophysical, photochemical and *in vitro* studies of **SiPcGal$_2$** are already published (45, 109), we have also used this SiPc in our studies for comparative purposes between the axial conjugation with protected-galacto-dendritic units (**SiPcGal$_4$**) and with protected-galactose molecules (**SiPcGal$_2$**). Studies with the commercially available **SiPc(OH)$_2$** were also performed in order to evaluate the Pc-core properties. **SiPc(OH)$_2$** was obtained by reacting $SiPcCl_2$ with sodium hydroxide (NaOH) in methanol (MeOH) at rt, during 30 min.

There are no reports of the removal of the isopropylidene groups from sugar moieties axially conjugated to SiPc. Thus, in those kind of compounds described in literature the researchers use a Cremophor EL emulsion for the *in vitro* assays that stabilize the solutions of nonpolar materials in aqueous systems, preventing their aggregation (45, 62, 63). Although this has not been applied to SiPcs, another

alternative to improve the hydrophilicity of a PS (*e.g.* ZnPc) is by its incorporation into liposomes (110). Additionally, studies with **SiPc(OH)$_2$** were performed on HeLa cells by incorporation of the PS inside the silica shell, in order to improve its dispersibility in aqueous environments (111). These are alternative strategies that could have been applied to the obtained compounds in the photobiological studies performed in this thesis.

It has to be taken into account that the idea of synthesizing a PS with affinity to the galactose-binding proteins overexpressed in cancer cells was unfortunately not accomplished because it was not possible to deprotect the galactose moieties of **SiPcGal$_4$** and **SiPcGal$_2$** thus preventing the interaction of the PS with those proteins. Therefore, the studies that will be further presented on this Master's thesis will be mostly to evaluate the promising properties of the SiPc core as well as the influence that axial substituents have in the Pc hydrophilicity.

Other routes can be performed to obtain the deprotected compounds, such as to deprotect first the galacto-dendritic units or the galactose molecules (112) and then axially conjugate them to the SiPc core. There are no papers that use that technique on SiPc, but it was reported the synthesis of a Por-glicopolymer based on a one-pot conjugation (combination of multi-reactions) (113) and also a gluco-conjugated ZnPc via Click reaction (generation of substances quickly and reliably by joining small units together) (114).

Part 2

Photophysical and photochemical studies of galacto-conjugates

2. Photophysical and photochemical studies of galacto-conjugates

In this section, photophysical and photochemical properties of **SiPcGal$_4$** and **SiPcGal$_2$** were determined and compared with those for **SiPc(OH)$_2$**. UV-Visible (UV/Vis) characterization, PSs solubility in organic and aqueous solvents, fluorescence properties and ability to generate $^1O_2$ were evaluated. These studies were performed at the University of Aveiro.

2.1 UV-Visible characterization, water solubility and fluorescence emission

The electronic absorption spectra of **SiPcGal$_4$**, **SiPcGal$_2$** and **SiPc(OH)$_2$** were initially acquired in the organic solvents DMF and dimethyl sulfoxide (DMSO). All the SiPcs at 10 μM gave typical UV/Vis spectra for non-aggregated SiPcs showing an intense and sharp Q band in the red visible region. That Q band was observed at 677, 669 and 667 nm for **SiPcGal$_4$**, **SiPcGal$_2$** and **SiPc(OH)$_2$**, respectively, and the Soret bands around 348 nm (**Figure 2.4**). To determine the solubility of these compounds in an aqueous buffered solution, their absorption spectra were also acquired in PBS (**Figure 2.4**). This study is a critical parameter for the PSs' PDT application, since in polar solvents, macrocycles have high aggregation tendency, disfavoring their efficacy as PDT agents (47). In PBS (3 % DMSO), the Q band of **SiPcGal$_4$** and **SiPcGal$_2$** undergo a significant broadening, which is a spectral feature of aggregated SiPcs. This feature was more evident for **SiPc(OH)$_2$** showing a higher aggregation of this compound. Therefore, these results demonstrated that the axial coordination increases the solubility of a SiPc in an aqueous solution, but to achieve strong hydrophilicity, the isopropylidene groups should be removed.

The extinction coefficients (ε) of the SiPcs in these three solvents are summarized in **Table 2.1**. The ε values of **SiPcGal$_2$** and **SiPc(OH)$_2$** in DMF and DMSO, respectively, are already described in literature (45,115), and are similar

with the ones described in this section. Comparing to others SiPcs axially conjugated with other protected sugars (*e.g.* glucose and cyclodextrin), the ε values in DMF were lower for **SiPcGal$_4$** and **SiPcGal$_2$** (62,63).

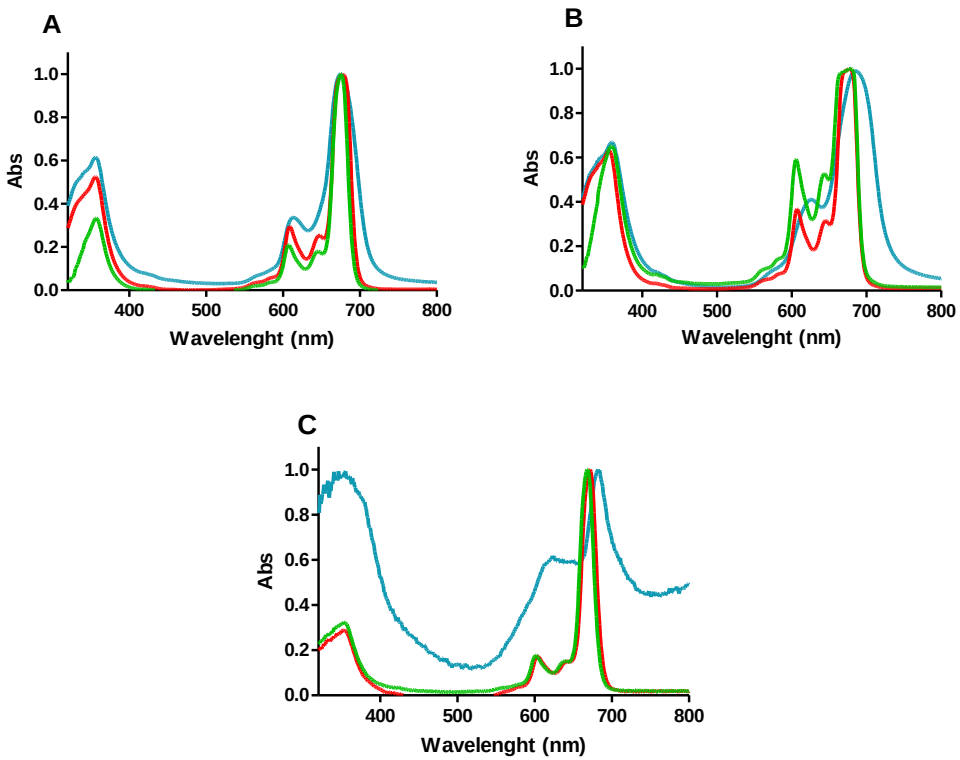

Figure 2.4. UV/Vis absorption spectra of **SiPcGal$_4$** (**A**), **SiPcGal$_2$** (**B**) and **SiPc(OH)$_2$** (**C**) at 10 μM in PBS (3 % DMSO, blue), DMF (green) and DMSO (red).

Once the biological studies were going to be performed in PBS, even knowing that the three SiPcs aggregated in this solvent, their maximum concentration to be used on cells was determined. UV/Vis studies with increasing concentrations of the compounds (0 to 10 μM) in PBS solution containing DMSO (up to 3%) showed that **SiPcGal$_4$** and **SiPcGal$_2$** strictly follow the Beer-Lambert law at the studied concentrations suggesting their application in *in vitro* studies at concentrations below 10 μM (**Figure 2.5**). The same did not happened with **SiPc(OH)$_2$,** because the absorbance at that concentration was very low and higher concentrations implied a percentage of DMSO higher than 3% (corresponding to 10 μM), which is not suitable for cellular assays. Previous assays performed by our group have

described that a percentage of DMSO higher than 0.5% significantly reduces the viability of human bladder cancer cells (UM-UC-3) (40,76), the same cells that we intended to use on the present study. Thus, even at a concentration of 10 µM, the percentage of DMSO was too high to be used. Therefore, only concentrations bellow 1.66 µM of **SiPcGal$_4$** and **SiPcGal$_2$** in PBS (% DMSO ≤ 0.5) could be used for the *in vitro* PDT assays without compromising their phototoxic effectiveness evaluation.

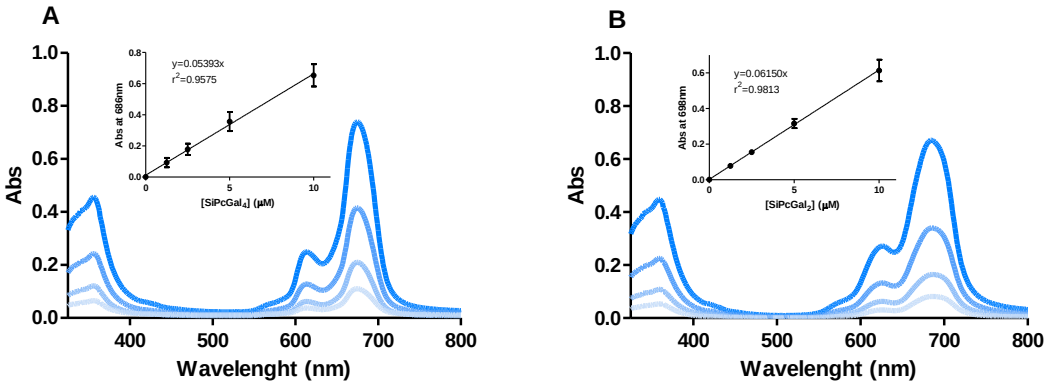

Figure 2.5. UV-Vis absorption spectra of **SiPcGal$_4$** and **SiPcGal$_2$** in PBS (**A** and **B**, respectively) at different concentrations (0 to 10 µM, % DMSO ≤ 3%). The inset plots of **SiPcGal$_4$** Q-band at 686 nm and **SiPcGal$_2$** Q-band at 698 nm *versus* concentration of the respective galacto-conjugate in PBS.

Additionally, the solubility of the SiPcs in DMF was also evaluated for the $^1O_2$ generation and fluorescence studies that were performed in this organic solvent. These studies were carried out with increasing concentrations of the compounds (up to 10 µM) in DMF solutions showing that **SiPcGal$_4$** and **SiPcGal$_2$** strictly followed the Beer-Lambert law only till 5 µM and 1.25 µM, respectively (**Figure 2.6**).

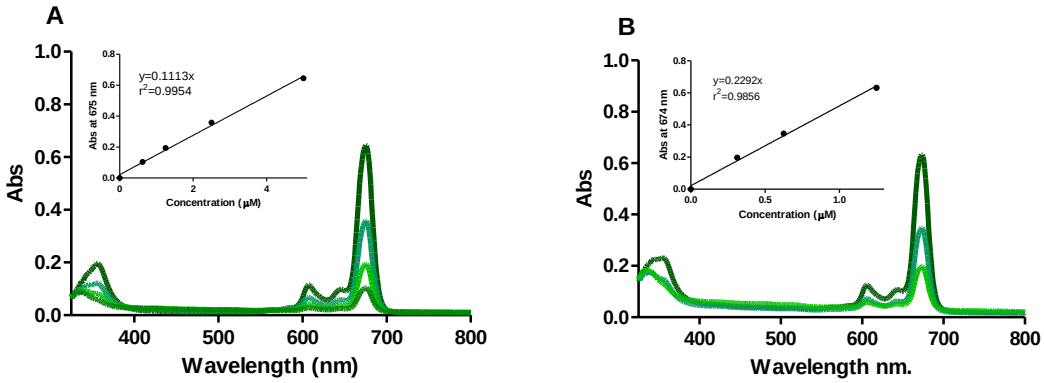

Figure 2.6. UV-Vis spectra of **SiPcGal$_4$** and **SiPcGal$_2$** in DMF at different concentrations (0 to 5 μM). The inset plots of **SiPcGal$_4$** Q-band at 675 nm and **SiPcGal$_2$** Q-band at 674 nm *versus* concentration of the respective galacto-conjugate in DMF.

The fluorescence emission of the PS provides information about its potential application in cancer diagnosis and therapeutics. The steady-state fluorescence emission spectra of **SiPcGal$_4$**, **SiPcGal$_2$** and **SiPc(OH)$_2$** were acquired in DMF. The three SiPcs demonstrated fluorescence emission bands in the red region of the spectrum (approximately between 680 and 750 nm, **Figure 2.7**) which can be used to determine the concentration of these PSs inside the cells or tissues.

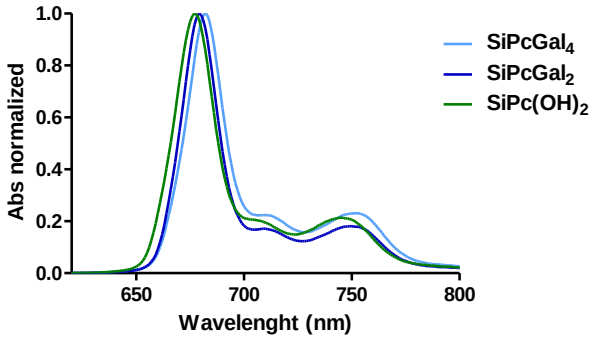

Figure 2.7 Normalized emission spectra of **SiPcGal$_4$**, **SiPcGal$_2$**, and **SiPc(OH)$_2$**.

Table 2.1. UV-Vis data of the galacto-conjugates in PBS, DMSO and DMF and of **SiPc(OH)$_2$** in DMSO and DMF.

Galacto-conjugate	Solvent	$\lambda_{absorption\ bands}$ [nm] (log ε)[a]	$\lambda_{emission}$ [nm]
SiPcGal$_4$	PBS	343 (4.31), 613 (4.00), 690 (4.50)	————
	DMSO	348 (4.00), 608 (3.95), 646 (3.84), 685 (4.26)	————
	DMF	369 (2.65), 607 (2.88), 646 (2.71), 679 (4.21)	682, 751
SiPcGal$_2$	PBS	340 (4.74), 627 (4.71), 698 (4.80)	————
	DMSO	326 (4.10), 607 (4.39), 647 (4.27) 683 (3.99)	————
	DMF	364 (3.25), 606 (3.94), 645 (3.92), 683 (4.29)	679, 750
SiPc(OH)$_2$	DMSO	354 (5.52), 605 (5.50), 672 (4.58)	————
	DMF	354 (2.71), 602 (2.62), 669 (3.85)	677, 746

[a]log ε $M^{-1}.cm^{-1}$

2.2 Singlet oxygen production

To evaluate the potential use of **SiPcGal$_4$** as a new PS for PDT, its ability to generate $^1O_2$ was evaluated in DMF. DPBF was used as $^1O_2$ scavenger (63). DPBF is a yellow colored compound with a maximum of absorption at 415 nm, that reacts with $^1O_2$ and it is oxidized to a colorless compound, the dibenzoylbenzene: thanks to this structural change, is possible to measure the scavenger absorption decay (116). The ability of **SiPcGal$_2$** and **SiPc(OH)$_2$** to generate $^1O_2$ was also determined, in order to evaluate the influence of the axial conjugation with dendritic units of galactose and the SiPc-core ability in the production of $^1O_2$. **SiPcGal$_4$**, **SiPcGal$_2$** and **SiPc(OH)$_2$** (0.3 µM), were able to photo-oxidize DPBF (30 µM) (**Figure 2.8**). Both galacto-conjugates demonstrated to be potent generators of $^1O_2$, once **SiPcGal$_4$** and **SiPcGal$_2$** were able to decompose 50% of DPBF after 15 min and 7 min of irradiation, respectively. The behavior of **SiPcGal$_2$** was similar to the one of **SiPc(OH)$_2$**. These results showed that the conjugation of SiPc with protected galactose moieties or galacto-dendritic units does not compromise the $^1O_2$ production. Therefore, these studies showed the promising ability of the SiPc-core itself in the generation of this ROS.

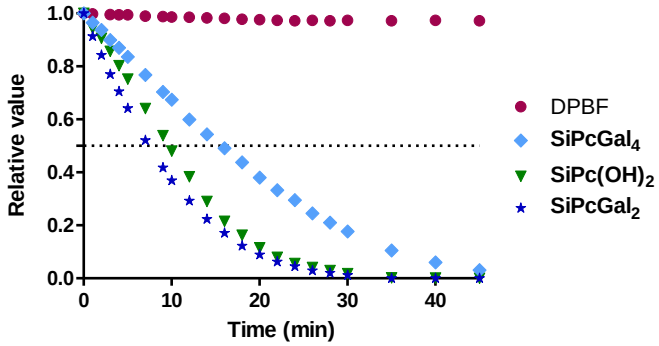

Figure 2.8. Photo-oxidation of DPBF (30 µM) in DMF with or without **SiPcGal$_4$**, **SiPcGal$_2$** or **SiPc(OH)$_2$** (0.3 µM), after irradiation with red light emitted by a LEDs array (λ > 600 nm, 5 mW.cm^{-2}). The DPBF absorbance was recorded at 415 nm.

2.3 Photostability of the galacto-conjugates

To evaluate the potentiality of the galacto-conjugates as new PSs, it is also important to determine their photostability when exposed to UV-Vis light and O_2. The intensity of the Q band of **SiPcGal$_4$**, **SiPcGal$_2$** and **SiPc(OH)$_2$** was monitored after irradiation with red light at a fluence rate of 150 mW.cm^{-2} (**Table 2.2**). These results demonstrated that the three SiPcs are photostable over the irradiation period of 30 min.

Table 2.2. Photostability of 20 µM of **SiPcGal$_4$**, **SiPcGal$_2$** and **SiPc(OH)$_2$** in PBS (6% DMSO), after irradiation with red light at a fluence rate of 150 mW.cm^{-2} for different periods of time (0-30 min). The results are presented in percentage calculated by the ratio of residual absorbance (at 683 nm) at different periods of time and absorbance before irradiation.

SiPc	Irradiation time (min)								
	0	1	3	4	5	10	15	20	30
SiPcGal$_4$	100	93	90	88	85	82	80	79	75
SiPcGal$_2$	100	98	94	94	94	94	94	94	94
SiPc(OH)$_2$	100	93	92	91	91	89	86	86	86

Part 3

In vitro studies of the galacto-conjugates

3. *In vitro* studies of the galacto-conjugates

3.1 Overview

Pcs are PSs with great photochemical and photophysical properties. Their coordination to a silicon atom reduces their aggregation, since its axial funcionalization with different bulky groups improves their solubility in a variety of solvents. This is directly connected to photosensitizing efficiency as well as fine-tune fluorescence and triplet state characteristics (52). In **Part 2** was possible to evaluate those properties, showing that **SiPcGal$_4$** and **SiPcGal$_2$** were good fluorescence labels; stable after light irradiation and efficient generators of $^1O_2$. However, as the deprotection of the isopropylidene groups of galactose was not achieved in those SiPcs, these compounds demonstrated reduced solubility in PBS. In **Part 3**, it will be evaluated the **SiPcGal$_4$** and **SiPcGal$_2$** potential as PSs in PDT based on uptake, phototoxicity and ROS production after PDT studies in a human bladder cancer cell line, UM-UC-3. The potential of **SiPcGal$_4$** and **SiPcGal$_2$** as PDT agents will be compared with the non-galacto-conjugated **SiPc(OH)$_2$**. UM-UC-3 cell line derives from transitional cell carcinoma, which is the most common malignant tumor arising from the urothelium. The morphology of these cells is defined by poorly adherent, displaying a stellate morphology (117). Additionally, UM-UC-3 BC cells exhibit high levels of a galactose-binding protein, galectin-1 (40).

These studies were performed at the Institute for Biomedical Imaging and Life Sciences (IBILI), Faculty of Medicine, University of Coimbra (FMUC).

3.2 Uptake of galacto-conjugates by UM-UC-3 bladder cancer cells

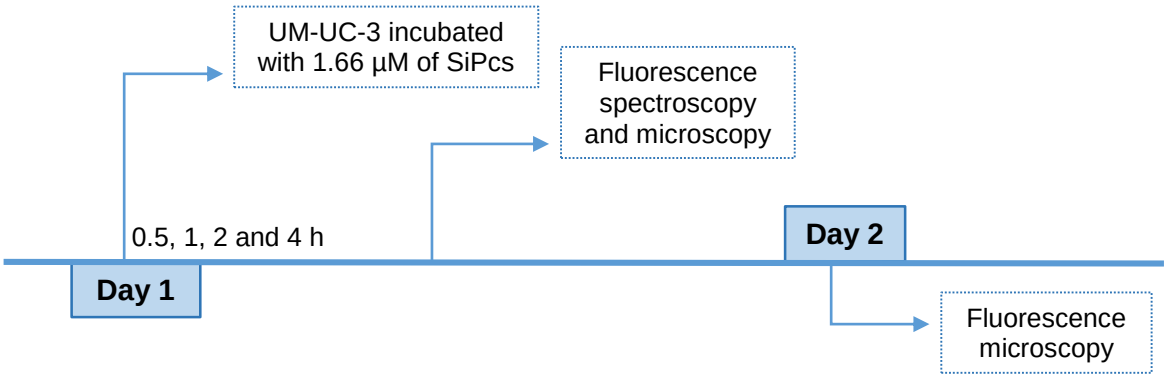

Scheme 2.5 Chronology of uptake studies performed after incubation of UM-UC-3 BC cells with **SiPcGal$_4$**, **SiPcGal$_2$** and **SiPc(OH)$_2$**.

Based on the fact that UM-UC-3 cells display high levels of Gal-1, we initially hypothesized that the presence of the galactose units could facilitate the entry of SiPcs into BC cells. However, as discussed in **Part 1**, galactose-protective groups were not successfully removed during their synthesis. Although this fact can compromise cellular uptake, we proceeded this work by performing their biological evaluation as potential photosensitizing agents for PDT. The BC cells UM-UC-3 were incubated with 1.66 µM SiPcs in the dark for different periods of time (up to 4 h) in PBS containing DMSO (less than 0.5%). The fluorescence properties of these compounds allowed the evaluation of their intracellular accumulation by quantitative spectrofluorimetry and fluorescence microscopy. Each SiPc had different fluorescence characteristics, which can be observed in the calibration slopes represented in section **3.2.3** of **Part 3** in **Methods and Materials**. The uptake of **SiPcGal$_2$** and **SiPcGal$_4$** was not dependent on the incubation time, probably due to their aggregation in PBS (as described in **Part 2** of **Results and Discussion**) as well as to their incapacity of interaction with galectin-1 thanks to the galactose-hydroxyl protective groups. Previous studies with a Pc containing eight dendritic units of galactose have demonstrated that its uptake in UM-UC-3 cancer cells is dependent on the concentration and reaches a plateau in less than 2 h (40). In the present study, the protected galactose molecules axially coordinated with SiPc did

not allow that uptake occurs in a both concentration- and uptake time dependent manner. Data showed that **SiPcGal$_4$** exhibited higher uptake than **SiPcGal$_2$** (**Figure 2.9**), but these results were inconclusive due to the high aggregation of both SiPcs in a PBS containing DMSO (less than 0.5%) solution. Comparing the three SiPcs, **SiPc(OH)$_2$** had the higher uptake which can be explained by a non-specific mechanism caused by reduction of the membrane permeability barrier towards amphiphilic **SiPc(OH)$_2$**. However, there are no records that can sustain this feature. Prior studies of **SiPcGal$_2$** in a Cremophor EL emulsion showed that this PS have high uptake and reaches a plateau after 2 h (45).

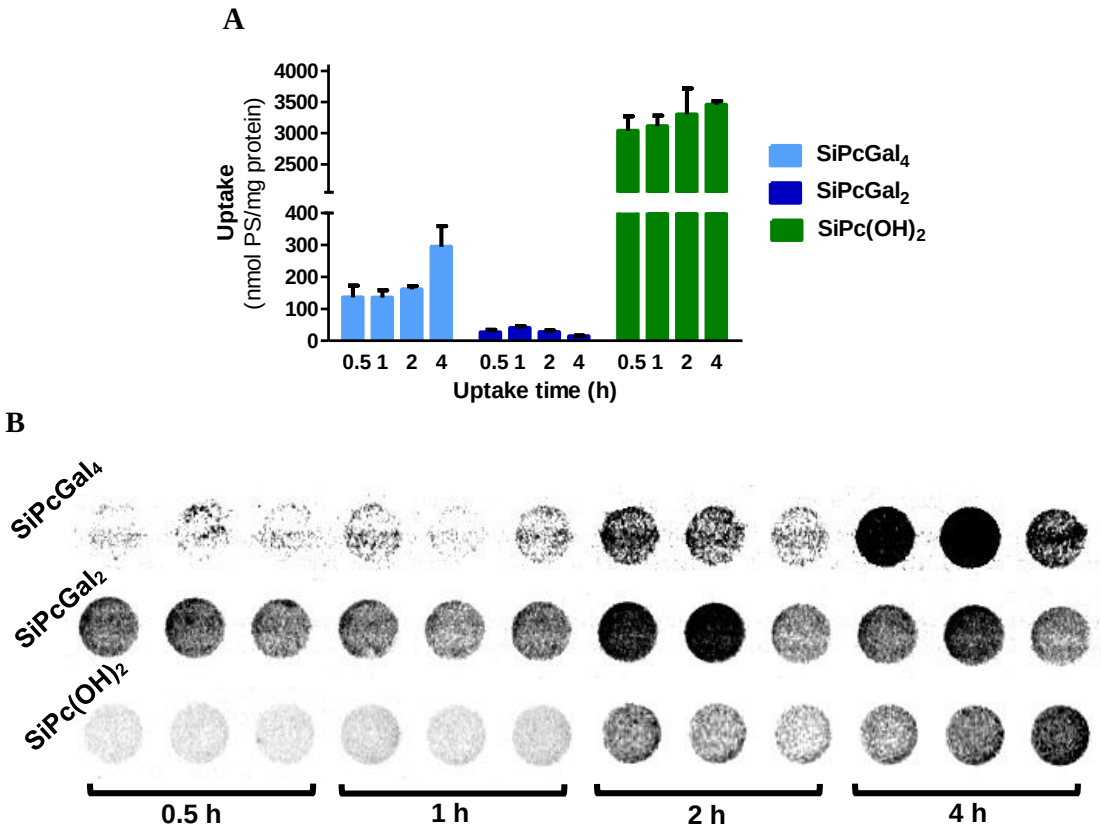

Figure 2.9. Intracellular accumulation of **SiPcGal$_4$**, **SiPcGal$_2$** and **SiPc(OH)$_2$** in UM-UC-3 cells. (**A**) Cellular uptake of **SiPcGal$_4$**, **SiPcGal$_2$** and **SiPc(OH)$_2$** (1.66 µM) by UM-UC-3 cells (in PBS containing 0.5% DMSO), normalized to protein quantity, in function of the uptake time (up to 4 h). (**B**) Representative raw data of fluorescence spectroscopy of BC incubated with 1.66 µM SiPcs in the dark, before the normalization to protein concentration. Each SiPc has different fluorescence characteristics (see calibration slopes in **3.2.3** of **Part 3** in **Methods and Materials**). Data are the mean ± SEM of two independent experiments performed in triplicates.

The intracellular accumulation of PSs by UM-UC-3 cancer cells was also determined by fluorescence microscopy (**Figure 2.10**). Cells were incubated with 1.66 µM of **SiPcGal$_4$**, **SiPcGal$_2$** and **SiPc(OH)$_2$** for 3 h (in darkness) and cell nuclei were stained with DAPI. The fluorescence of the three PSs was remarkable. Fuorescence microscopy confirmed the spectrofluorimetric data showing that cells incubated with the three SiPc exhibit occasional bright spots in the perinuclear region. Apparently, for both **SiPcGal$_4$** and **SiPcGal$_2$** red spots were found outside the cells (**Figure 2.10, A** and **B**), suggesting aggregation of the two galacto-conjugates. However, acquisition of fluorescence images in bright field could help to confirm the intracellular accumulation of the SiPc. Contrary to the other two SiPc, **SiPc(OH)$_2$** was found throughout the cytoplasm of cancer cells, showing co-localization with the nuclei (**Figure 2.10, C**). This could be due to its amphilicity relatively to the other two PSs.

Previous studies of intracellular fluorescence of **SiPcGal$_2$** in a Cremophor EL emulsion showed that this Pcs exhibit a co-localization with mitochondria (stained with MitoTracker Green FM dye), but not in a exclusively way (45). It would be interesting to determine the intracellular location of the three SiPcs using organelle-specific dyes.

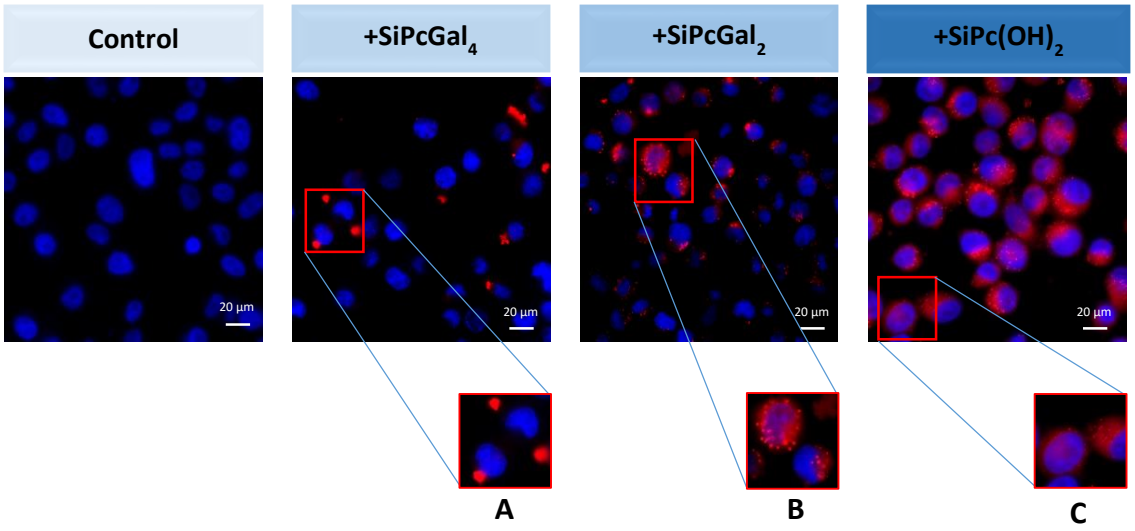

Figure 2.10. Representative fluorescence images of UM-UC-3 cells incubated with 1.66 µM of **SiPcGal$_4$**, **SiPcGal$_2$** and **SiPc(OH)$_2$** for 3 h in darkness (red) with nucleus stained with DAPI (blue). Control fluorescence images (without PS fluorescence) were acquired after cells´ incubation with PBS for 3 h in the dark and staining the nucleus with DAPI (blue). Scale bars, 20 µm, are indicated on images. Original magnification: 60x. Insets images of the three PSs are also represented (**A**, **B** and **C**).

3.3 Dark toxicity and phototoxicity determination of galacto-conjugates in UM-UC-3 bladder cancer cells

A good PS has to be non-toxic until activation by light at a specific wavelength. Thus, after confirming the uptake of PSs by UM-UC-3 cancer cells, PSs cytotoxicity in darkness was determined. UM-UC-3 cells were incubated with increasing concentrations of PSs (0.05 - 1.66 µM) in PBS (containing less than 0.5% DMSO) in darkness for 3 h. Cell viability was determined 24 h after treatment by MTT colorimetric assay, where the yellow-colored MTT is reduced by mitochondrial dehydrogenases in living cells to a formazan precipitate. The formazan absorbance is directly correlated with the metabolic activity of living cells. **SiPcGal$_4$**, **SiPcGal$_2$** and **SiPc(OH)$_2$** up to 1.66 µM did not induce significant dark toxicity (**Figure 2.11**).

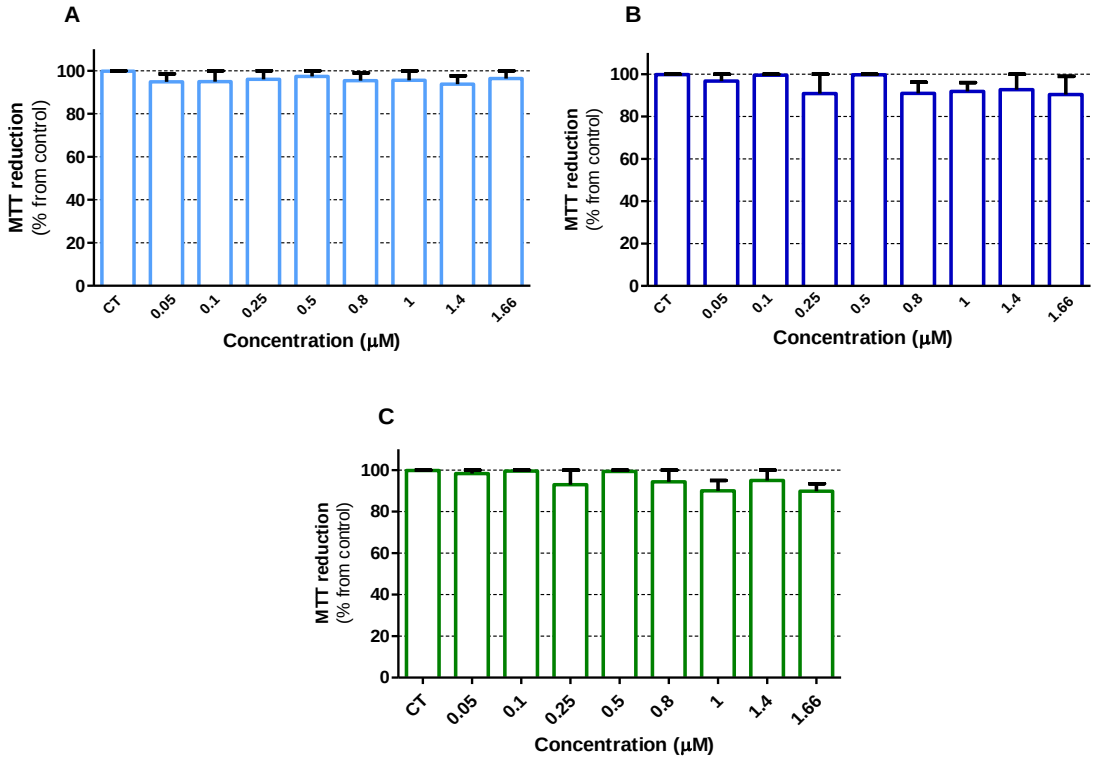

Figure 2.11. **SiPcGal$_4$** (**A**), **SiPcGal$_2$** (**B**) and **SiPc(OH)$_2$** (**C**) cytotoxicity in the dark in UM-UC-3 cells. PSs were incubated with different concentrations (0.05 - 1.66 µM, DMSO up to 0.5%) in UM-UC-3 cells. Cytotoxicity was assessed using MTT colorimetric assay 24 h after treatment. The percentage of cytotoxicity was calculated relatively to control cells (cells incubated with PBS in darkness). Data are the mean value ± SEM of two independent experiments performed in triplicates.

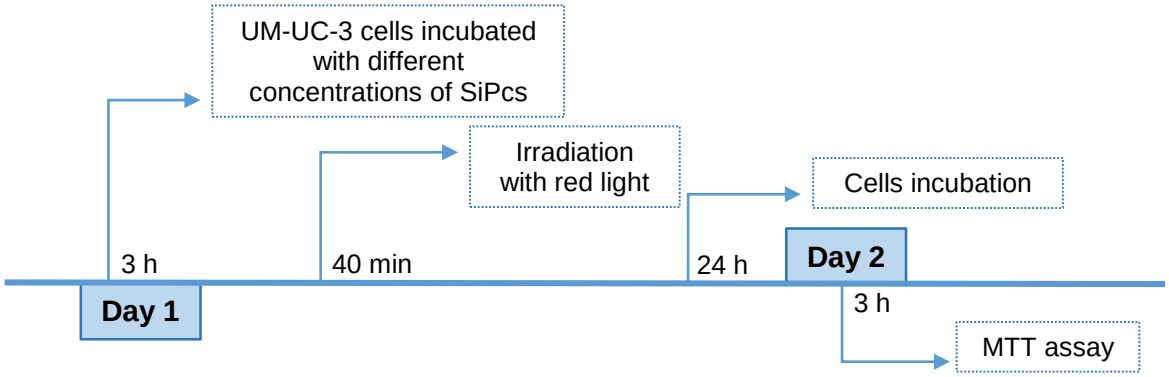

Scheme 2.6 Chronology of PDT studies of **SiPcGal$_4$**, **SiPcGal$_2$** and **SiPc(OH)$_2$** in UM-UC-3 BC cells.

After confirmation of no dark toxicity of the three PSs, the effect of light irradiation after **SiPcGal$_4$**, **SiPcGal$_2$** and **SiPc(OH)$_2$** uptake on cell viability, MTT was performed 24 h after treatment. After PSs uptake in darkness, cells were irradiated with red light at a potency of 2.5 mW.cm^{-2} for 40 min. Control experiments using irradiated cells (previously incubated with PBS (containing 0.5% DMSO) for 3 h in the dark) were performed, in order to determine the effect of red light irradiation alone on cell viability. These conditions did not induce toxicity in the cells. However, in the presence of the PSs, there was an increase of the phototoxicity dependent on the PS concentration.

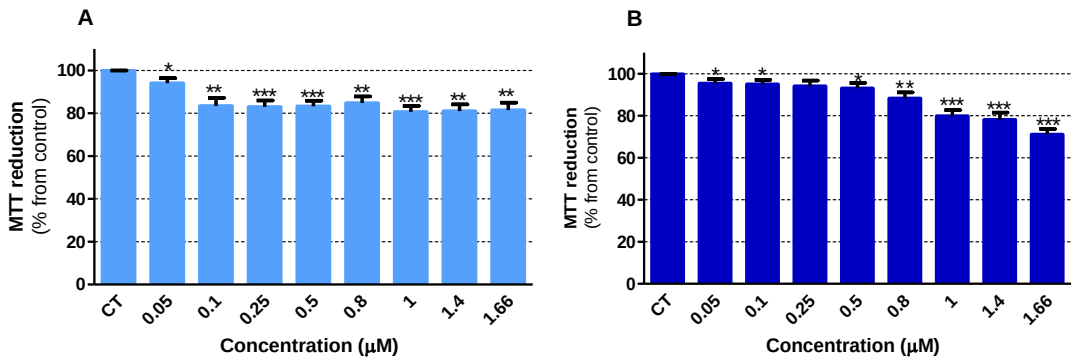

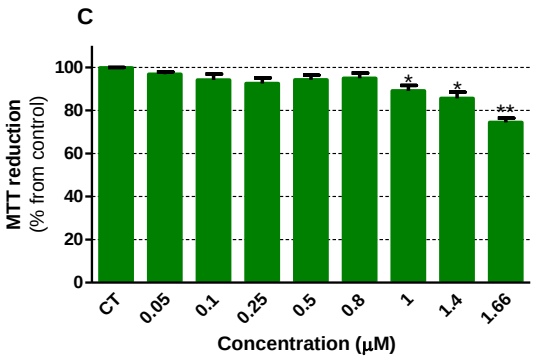

Figure 2.12. Photocytotoxic effect after SiPc-PDT in UM-UC-3 cells evaluated 24 h after PDT. UM-UC-3 BC cells were incubated with increasing concentrations (0.05 - 1.66 µM) of **SiPcGal$_4$** (**A**), **SiPcGal$_2$** (**B**) and **SiPc(OH)$_2$** (**C**) for 3 h, in the dark, and then irradiated with white light at a fluence rate of 2.5 mW.cm^{-2} for 40 min. Cytotoxicity was assessed using MTT colorimetric assay 24 h after treatment. The percentage of cytotoxicity was calculated relatively to control cells (cells incubated with PBS (containing up to 0.5% DMSO) for 3 h in darkness and then irradiated). Data are the mean value ± SEM of two independent experiments performed in triplicates. *($p < 0.05$), **($p < 0.001$), ***($p < 0.0001$) significantly different from control cells.

Among these conditions, **SiPcGal$_4$**, **SiPcGal$_2$** and **SiPc(OH)$_2$** presented similar ability to induce cell death after PDT with a percentage of toxicity of 18.52, 28.77 and 26.72 %, respectively, at 1.66 µM. It is expected that only the non-aggregated fraction of each SiPc would be able to induce cell death, though it is necessary to perform this study at higher concentrations or in bio-stable formulations. Comparing these results with the ones described in literature, the PSs phototoxicity was promising considering the aggregation problem. PcGal$_{16}$ (Pc containing eight deprotected dendritic units of galactose), within the same conditions, after 2 h of uptake and at a PS concentration between 0.5 and 2.5 µM, the percentage of toxicity was of approximately 50% (2x higher than the SiPcs toxicity) (40), showing the great potential of these galacto-conjugated SiPcs to be studied in new approaches where the aggregation issue is resolved. Nevertheless, these results cannot be compared to the ones of **SiPcGal$_2$** in a Cremophor EL emulsion, because the conditions were very different: irradiation potency of 40 mW.cm^{-2} (16 x higher) and they only used half of the irradiation time. Those results showed that a much lower concentration of **SiPcGal$_2$** (0.10 µM) was able to decrease cell viability by 50% (45).

3.4 $SiPcGal_4$, $SiPcGal_2$ and $SiPc(OH)_2$ induced reactive oxygen species production after PDT in UM-UC-3 bladder cancer cells

Since it is well established that ROS production has an important role in PDT-induced cell death, the intracellular production of ROS was evaluated immediately after PDT in cells previously incubated with 1.66 µM of the three SiPc for 3 h. In order to correlate the PSs' phototoxicity with ROS production, three different ROS-sensitive probes: DHE, H_2DCFDA and MiyoPy1 (118-120) were used. DHE is able to react with $O_2^{\cdot -}$ and be oxidized to ethidium, which intercalates within the cell's DNA, staining the nucleus with bright red fluorescence. H_2DCFDA reacts with several cytotoxic ROS leading to the formation of the fluorescence compound DCF. Finally, MitoPy1 selectively tracks to the mitochondria and responds to local fluxes of H_2O_2 by a turn on fluorescence enhancement.

First, UM-UC-3 cells were incubated for 3 h with PBS (control) or 1.66 µM of **$SiPcGal_4$**, **$SiPcGal_2$** and **$SiPc(OH)_2$**, in darkness and then they were irradiated for 40 min. None of the SiPcs tested induced a high production of ROS after PDT (**Figure 2.13**). Regarding **$SiPcGal_4$**, this PS did not showed an increase in the $O_2^{\cdot -}$ production, but the generation of H_2O_2 and total ROS was significant. **$SiPcGal_2$** and **$SiPcOH_2$** showed, after PDT, a significant increase in the production of $O_2^{\cdot -}$, H_2O_2 and total ROS. Once again, it is expected that only the non-aggregated fraction of each SiPc would be able to produce ROS, though it is necessary to perform this study at higher concentrations or in bio-stable formulations. **$SiPcGal_2$** in a Cremophor EL emulsion showed high production of ROS levels as determined using DCFDA probe (109).

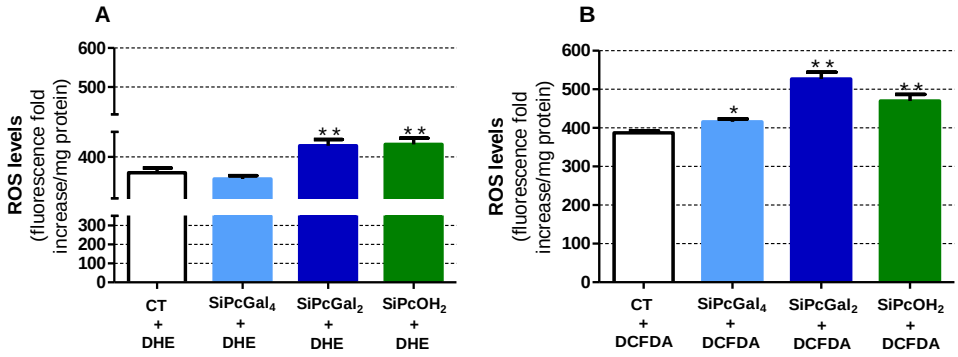

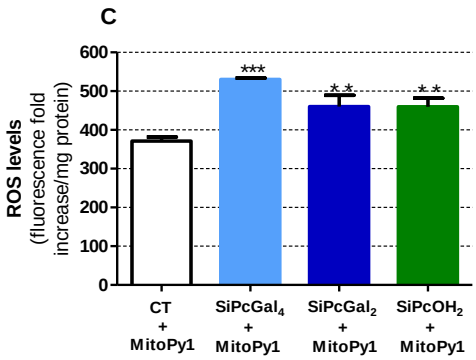

Figure 2.13. Quantification of DHE (**A**), DCF (**B**) and MitoPy1 (**C**) fluorescence increase (as a measure of ROS production) after PDT with **SiPcGal$_4$**, **SiPcGal$_2$** and **SiPc(OH)$_2$**. UM-UC-3 cells were incubated with PBS (control) or 1.66 µM of **SiPcGal$_4$**, **SiPcGal$_2$** or **SiPc(OH)$_2$** for 3 h in the dark. After PDT during 40 min, the fluorescent signals of the probes were quantified by fluorescent spectroscopy. Data are the mean value ± SEM of two independent experiments performed in triplicates. *($p < 0.05$), **($p < 0.001$), ***($p < 0.0001$) significantly different from control cells.

CHAPTER III

CONCLUSION AND FUTURE PERSPECTIVES

III. Conclusions and future perspectives

In this Master's dissertation, we attempted the synthesis of symmetrical water soluble SiPcs axially coordinated with galacto-dendritic units. We also aimed the removal of the isopropylidene galactose-protective groups from the already described in the literature, SiPc axially conjugated with two galactose moieties (**SiPcGal$_2$**), so that we can have a comparative compound. These galactose molecules will be recognized by galectins (galactose-binding proteins), overexpressed in bladder tumors. Thus, after the drug design, the following step was to study their photophysical and photochemical properties, and to validate them as photodynamic therapeutic agents against BC cells.

The preparation of the two SiPc axially conjugated with galacto-dendritic units was partially achieve once it was only possible to perform the coordination step of the SiPc dichloride ($SiPcCl_2$) with the protected galacto-dendritic units containing the 1,3-propanediol chain (**SiPcGal$_4$**). Additionally, our several attempts to hydrolyze the isopropylidene groups of the galactose molecules in either the **SiPcGal$_4$** or **SiPcGal$_2$** failed. However, a new galacto-dendritic unit [**3**] was obtained and in future work, different approaches could be used to then produce the desired final PS. One methodology that can be applied is to first hydrolyze the isopropylidene groups of compound **3**, with TFA/water (9:1) and then conjugate it with the $SiPcCl_2$ in a reflux DMF reaction. Other route than we can undergo is to hydrolyze the isopropylidene groups of compound **1** and then conjugate it with **SiPc(OH)$_2$** in a reflux DMF reaction with potassium carbonate (K_2CO_3). Finally, to obtain **SiPcGal$_2$** with the deprotected galactose molecules, we can conjugate the commercially available D-(+)-galactose with $SiPcCl_2$ also in a reflux DMF reaction with K_2CO_3. However, it is possible that we will be confronted with solubility issues to perform these reactions.

Regarding the photophysical and photochemical studies, both galacto-conjugates were also compared with SiPc dihydroxide (**SiPc(OH)$_2$**) in order to understand if the SiPc core properties are useful for future drug design. **SiPcGal$_4$**

and **SiPcGal$_2$** containing the isopropylidene groups demonstrated some particular properties that allowed us to predict the behavior of these macrocyclic cores. Of course there were some issues on their hydrophilicity under physiological conditions, which are fundamental for drug administration. Yet, in comparison with the **SiPc(OH)$_2$**, their water solubility was higher due to the presence of axial substituents that reduced their aggregation. Thus, if the isopropylidene goups' hydrolysis was successfully accomplished, the solubility would be much higher. The typical spectra of this SiPcs contained a strong Q-band absorption at around 670 nm (therapeutic window), which allows deeper tissue penetration upon light irradiation. Both PSs also demonstrated to be good $^1O_2$ generators and photostable upon 30 min of irradiation, which showed their high capacity to be used as PDT agents. Determination of the galacto-conjugates affinity to HSA and galectin-1 proteins could be an interesting approach to perform if we were successful in the hydrolysis of the galactoses' protective groups. HSA is a blood protein that is able to transport many drugs to the effector place demonstrating their ADME properties and galectin-1 is a galactose-binding protein overexpressed in BC cells.

For the *in vitro* photodynamic assays, a human bladder cancer cell line, UM-UC-3, derived from the transitional cell carcinoma of the bladder was used. The uptake of the two galacto-conjugates was lower than the uptake of the **SiPc(OH)$_2$**. This feature resulted from non-specific mechanism caused by reduction of the membrane permeability barrier towards amphiphilic **SiPc(OH)$_2$**. However, the PSs uptake was not correlated with the concentration and incubation time increment, due to their high aggregation in PBS solution, leaving the results inconclusive. The fluorescence microscopy study suggested that aggregation outside of the cells may occur, but on the other hand, it was clear their outstanding fluorescence properties.

SiPcGal$_4$ and **SiPcGal$_2$** were non-toxic in the dark but after photoactivation, they induced a significant decrease in cell viability. However, once these SiPcs aggregate in cells, it was expected that only a fraction of the administered Pc (non-aggregated fraction) will induce cell death, thus being difficult to interpret these results.

The PSs-induced ROS after PDT were also studied and showed an increase of the H_2O_2 present in the mitochondria and also of other general ROS in the cytoplasm. If these results were from the deprotected **SiPcGal$_4$** and **SiPcGal$_2$**, the next step could be studies of fluorescence microscopy using different fluorescent probes to study co-localization of the new PSs with different organelles. Another study that could be performed if we had the desired compounds, is the immunofluorescence staining of Gal-1 to observe the subcellular localization of this lectin and the galacto-conjugates in BC cells, and their possible co-localization. Specific inhibition of galectin-1 expression by RNAi (interference ribonucleic acid) could also be an approach to be used in future works, in an attempt to investigate the involvement of this protein in the uptake of the PSs BCa cells.

CHAPTER IV

METHODS AND MATERIALS

Part 1

Synthesis of galacto-phthalocyanines

1. Synthesis of galacto-phthalocyanines

1.1 Equipment, materials and reagents

1.1.1 Equipment and materials

Flash column chromatography was carried out with silica gel Merck-60 (230-400 mesh, 0.040-0.063 mm) and size exclusion chromatography by Biorad, Biobeads SX-1. Analytical Thin Layer Chromatography (TLC) on pre-coated sheets with silica gel 60 F254 or 60 ReversePhase-18 F254 S were from Merck. Reverse phase column chromatography was carried out using Sep-Pak®Vac 35 cc (10 g) columns.

NMR spectra (^{1}H and ^{13}C) were recorded with a Bruker AV-300 (300 MHz) instrument. Deuterated solvents used are indicated in brackets and tetramethylsilane (TMS) was used as internal reference. The chemical shifts (δ) are expressed in ppm and the coupling constants (*J*) in Hz. Maldi-MS were obtained in positive ion mode from an Applied Biosystem 4700 instrument or a Bruker Ultraflex III TOFTOF both equipped with a Nd:YAG laser operating at 355 nm and were carried out at *Servicio Interdepartamental de Investigación* (SIdI) of the University Autónoma of Madrid.

1.1.2 Reagents and chemical products

$SiPcCl_2$, 1,2:3,4-di-O-isopropylidene-α-D-galactopyranose, 1,3-propanediol, 1,3-dimercaptopropane, TCT, NaH and pyridine were obtained from Sigma-Aldrich.

DMF, DCM, Hex, AcOEt, tetrahydrofuran (THF), MeOH, DIPEA and toluene were purchased from Fisher Scientific.

TFA and TMSBr are from Tokyo Chemical Industry (TCI) and sodium bicarbonate ($NaHCO_3$) from Merck.

1.1.3 Software

ChemDraw Ultra 14.00 from CambridgeSoft was the software used to draw the chemical structures. MestReNova LITE was used to analyze the ^{1}H and ^{13}C NMR spectra.

1.2 Experimental procedures

1.2.1 Galacto-dendritic units synthesis

A. Synthesis of 2-chloro-4,6-bis(1,2:3,4-di-O-isopropylidene-α-D-galactopyran-6-yl)-1,3,5-triazine [**1**] (72)

Compound **1** (2-chloro-4,6-bis(1,2:3,4-di-O-isopropylidene-α-D-galactopyran-6-yl)-1,3,5-triazine) was synthesized as previously described in literature. 1,2:3,4-di-O-isopropylidene-α-D-galactopyranose (3.0 g, 11.60 mmol) was dissolved in dry toluene (30 mL) and a large excess of DIPEA (4.0 mL) was added. The reaction was then cooled at 0 ºC and TCT (1.1 g, 5.80 mmol) was added to the mixture. The reaction was stirred at 60 ºC during 72 h, under Ar. After concentration under vacuum, the residue was purified by flash gradient column chromatography on silica gel, by using Hex:AcOEt (8:2 to 7:3 v/v) as eluent, affording compound **1** as a white solid (2.43 g, 66%). **^{1}H NMR** (300 MHz, $CDCl_3$): δ 1.31, 1.32, 1.44 and 1.49 (4s, 4 x 6H, CH_3), 4.18 (ddd, 4H, $J_{4'\text{-}5'}$= 1.4, $J_{5'\text{-}6'a}$ = 6.4, $J_{5'\text{-}6'b}$ = 6.5 Hz, H-5'), 4.30 - 4.33 (m, 4H, H-2', H-4'), 4.53 (m, 4H, H-6'a and H-6'b), 4.62 (dd, 4H, $J_{2'\text{-}3'}$ = 7.9, $J_{3'\text{-}4'}$ = 2.4 Hz, H-3') and 5.52 (d, 2H, $J_{1'\text{-}2'}$ = 5.0 Hz, H-1') ppm.

B. Synthesis of 3-[(4,6-bis(1,2:3,4-di-O-isopropylidene-α-D-galactopyran-6-yl)-1,3,5-triazin-2-yl)thio]propane-1-thiol [**2**] (72)

Compound **2** (3-[(4,6-bis(1,2:3,4-di-O-isopropylidene-α-D-galactopyran-6-yl)-1,3,5-triazin-2-yl)thio]propane-1-thiol) was synthesized as previously described in literature. Compound **1** (0.50 g, 1.58 mmol) was dissolved in dry toluene (9.0 mL). DIPEA (0.69 mL, 7.90 mmol) and 1,3-dimercaptopropane (0.25 mL, 6.32 mmol) were then added and the mixture stirred at 70 ºC during 48 h, under Ar. After concentration under reduced pressure, the residue was purified by column chromatography on silica gel, using a mixture of Hex/AcOEt (7:3 to 6:4 v/v) as eluent. The desired compound **2** was obtained as a viscous colorless oil (0.44 g, 89%). **^{1}H NMR** (300 MHz, $CDCl_3$): δ 1.31, 1.32, 1.44 and 1.49 (4s, 4 x 6H, CH_3), 2,02 (m, 2H, $CH_2\underline{CH_2}CH_2SH$), 2.64 (m, 2H, $CH_2CH_2\underline{CH_2}SH$), 2.75-2.80 (m, 1H, SH), 3.23 (m, 2H, $\underline{CH_2}CH_2CH_2SH$), 4.17 (ddd, 4H, $J_{4'\text{-}5'}$= 1.7, $J_{5'\text{-}6'a}$ = 4.8, $J_{5'\text{-}6'b}$ = 6.9 Hz, H-5'), 4.30-4.34 (m, 4H, H-2', H-4'), 4.50 (m, H-6'a and H-6'b), 4.61 (dd, 4H, $J_{2'\text{-}3'}$ = 7.7, $J_{3'\text{-}4'}$ = 2.3 Hz, H-3') and 5.52 (d, 2H, $J_{1'\text{-}2'}$ = 4.7 Hz, H-1') ppm. **MS** (ESI+, MeOH + 0.1% formic acid) results were: *m/z* calculated for $C_{30}H_{45}N_3O_{12}S_2$ $[M+H]^+$: 704.24 found: 704.25.

C. Synthesis of 3-[(4,6-bis(1,2:3,4-di-O-isopropylidene-α-D-galactopyran-6-yl)-1,3,5-triazin-2-yl)oxi]propane-1-diol [**3**]

Under Ar, compound **1** (720 mg, 1.14 mmol) was dissolved in dry toluene (9.0 mL) and then it was added DIPEA (0.55 mL, 5.72 mmol) and 1,3-propanediol (0.46 mL, 5.72 mmol). The mixture was stirred at 80 ºC during 72 h. After concentration under vacuum, the residue was purified by column chromatography on silica gel, using a mixture of Hept:AcOEt (6:4 to 1:1 v/v) to afford compound **3** (471 mg, 61%) as a viscous yellow oil. **^{1}H NMR** (300 MHz, $CDCl_3$): δ 1.31, 1.32, 1.44 and 1.49 (4s, 4 x 6H, CH_3), 1.99 (m, 2H, $CH_2\underline{CH_2}CH_2OH$), 3.76 (m, 2H, $CH_2CH_2\underline{CH_2}OH$), 4.18 (ddd, 2H, $J_{4'\text{-}5'}$= 1.8, $J_{5'\text{-}6'a}$ = 6.5, $J_{5'\text{-}6'b}$ = 6.6 Hz, H-5'), 4.30-4.35 (m, 4H, H-2', H-4'), 4.51 (m, 4H, H-6'a and H-6'b), 4.54 (m, 2H, $\underline{CH_2}CH_2CH_2OH$), 4.61 (dd, 4H, $J_{2'\text{-}3'}$ = 8.4, $J_{3'\text{-}4'}$ = 2.4 Hz, H-3') and 5.52 (d, 2H, $J_{1'\text{-}2'}$ = 5.0 Hz, H-1') ppm. **MS** (ESI+, MeOH

+ 0.1% formic acid) results were: *m/z* calculated for $C_{30}H_{45}N_3O_{14}$ $[M+H]^+$: 672,29 found: 672.30.

1.2.2 Coupling of $SiPcCl_2$ with galacto-dendritic units

A. Synthesis of SiPc **4** [**$SiPcGal_2$**] (45)

$SiPcGal_2$ was afforded following a procedure described in the literature by reacting $SiPcCl_2$ (163 mg, 0.225 mmol) with 1,2:3,4-di-O-isopropylidene-α-D-galactopyranose (118 mg, 0.454 mmol) and NaH (67 mg, 0.897 mmol). The reaction mixture was put in toluene reflux at 120 ºC during 48 h, under Ar. After concentration under vacuum, the crude product was purified by column chromatography on silica gel using a mixture of Hex/AcOEt (7:3 v/v) as eluent and then collected as a blue solid (126 mg, 53%). **^{1}H NMR** (300 MHz, $CDCl_3$): δ -2.37 (dd, 2H, *J* = 8.8, 9.3 Hz, OCH), -1.70 (dd, 2H, *J* = 5.3, 8.3 Hz, OCH), 0.30 (s, 6H, Me), 0.49 (s, 6H, Me), 0.68 (virtual s, 8H, Me and H-5'), 0.76 (dd, 2H, *J* = 1.0, 8.2 Hz, H-4'), 0.79 (s, 6H, Me), 3.22 (dd, 2H, *J* = 1.5, 8.5 Hz,H-3'), 3.32 (dd, 2H, *J* = 1.6, 5.4 Hz, H-2'), 4.37 (d, 2H, *J* = 5.0 Hz, H-1'), 8.28-8.31 (m, 8H, Pc–$H_β$) and 9.59-9.62 (m, 8H, Pc–$H_α$) ppm. **MS** (MALDI, DCTB+NaI) results were: *m/z* calculated for $C_{56}H_{54}N_8O_{12}Si$ $[M]^+$: 1058.4 found: 1058.4.

B. Failed attempt of synthesis of SiPc **5**

The $SiPcCl_2$ (30 mg, 0.049 mmol) and dendritic unit **2** (100 mg, 0.142 mmol) were dissolved in DMF (2.5 mL), and the reaction stirred at 120 ºC for 24 h, under Ar. After evaporating the solvent the crude product was purified by column chromatography using DCM/Hex (3:1 to 1:0 v/v) and then DCM/MeOH (80:1 to 60:1 v/v) as eluents. The collected fraction was further purified by BioBeads (DCM). The obtained product had a blue color. The ^{1}HNMR spectrum didn't show any sugar characteristic signals and **MS** (MALDI, DCTB+NaI) results were: *m/z* calculated for $C_{92}H_{104}N_{14}O_{24}S_4Si$ $[M+H]^+$: 1946 found: 574 (**$SiPc(OH)_2$**).

C. Synthesis of SiPc **6** [**SiPcGal$_4$**]

SiPcGal$_4$ was prepared by a reaction between $SiPcCl_2$ (67 mg, 0.0934 mmol), compound **3** (300 mg, 0.447 mmol) and a large excess of pyridine (0.2 mL). The compounds were dissolved in 12 mL of toluene and the mixture refluxed overnight. After elimination of the solvent under vacuum, the residue was purified by column chromatography on silica gel Hex:AcOEt (3:2 to 1:1 v/v) affording **SiPcGal$_4$** as a blue solid (30 mg, 12%). **^{1}H NMR** (300 MHz, $CDCl_3$): δ -1.99 (t, 4H, J = 6.5 Hz, $CH_2CH_2\underline{CH_2}OSi$), -1.06 (m, 4H, $CH_2\underline{CH_2}CH_2OSi$), 0.00 (t, 6H, J = 3.9 Hz, $\underline{CH_2}CH_2CH_2OSi$), 1.38, 1.41, 1.54 and 1.55 (4s, 4 x 12, CH_3), 4.22 (ddd, 4H, 8H, $J_{4'-5'}$= 1.0, $J_{5'-6'a}$ = 4.0, $J_{5'-6'b}$ = 4.0 Hz, H-5'), 4.32 (m, 4H, H-4'), 4.39 (m, 4H, H-2'), 4.42 (m, 8H, H-6'), 4.69 (dd, 4H, $J_{2'-3'}$ = 4.7, $J_{3'-4'}$ = 1.4 Hz, H-3'), 5.64 (d, 4H, $J_{1'-2'}$ = 2.9 Hz, H-1'), 8.29-8.31 (m, 8H, Pc–H$_\beta$) and 9.55-9.57 (m, 8H, Pc–H$_\alpha$) ppm. **^{13}C NMR** ($CDCl_3$): δ 24.5, 25.0, 26.1 and 26.2 (Me-isop), 27.8 ($CH_2\underline{CH_2}CH_2OSi$), 52.6 ($CH_2CH_2\underline{CH_2}OSi$), 65.5 ($\underline{CH_2}CH_2CH_2OSi$), 66.0 (C-5'), 70.7 (C-6'), 76.8 (C-3'), 77.0 (C-2'), 77.3 (C-4'), 96.4 (C-1'), 96.4, 107.9, 108.8, 109.5, 114.4, 123.6, 129.7, 130.9, 131.0, 135.8, 137.7 (Pc-C$_\beta$), 139.1, 139.5, 140.1, 149.2 (Pc-C$_\alpha$), 165.3 (C-4, C-6, TCT) and 172.2 (C-2, TCT) ppm. **MS** (MALDI, DCTB) results were: *m/z* calculated for $C_{92}H_{104}N_{14}O_{28}Si$ $[M+H]^+$:1881.7 found: 1881.6.

1.2.3 Failed attempts of deprotection of the isopropylidene groups

A. Deprotection of isopropylidene groups in **SiPcGal$_4$** and **SiPcGal$_2$** using TFA/water (9:1)

SiPcGal$_4$ (20 mg, 0.0189 mmol) and **SiPcGal$_2$** (20 mg, 0.0106 mmol) in TFA/water (9:1 v/v, 5 mL) were stirred at rt during 5 h. The mixture was neutralized with an aqueous solution of $NaHCO_3$ (pH=7.0) and the product was purified by reverse phase column chromatography on silica gel (THF/H_2O, 7:3 v/v) as eluent. Both compounds were then precipitated with DCM, filtered, washed with acetone and dried under reduced pressure.

Deprotected SiPcGal$_2$ MS (MALDI, DCTB+NaI) results were: *m/z* calculated for $C_{44}H_{38}N_8O_{12}Si$ $[M]^+$: 898.2, found: 574.2 (**SiPc(OH)$_2$**).
Deprotected SiPcGal$_4$ MS (MALDI, DCTB+NaI) results were: *m/z* calculated for $C_{68}H_{72}N_{14}O_{28}Si$ $[M]^+$: 1560.4, found: 574.2 (**SiPc(OH)$_2$**).

B. Deprotection of isopropylidene groups in **SiPcGal$_4$** and **SiPcGal$_2$** using TMSBr

SiPcGal$_4$ (10 mg, 0.0473 mmol) and **SiPcGal$_2$** (10 mg, 0.00531 mmol) were dissolved in DCM and then it was added TMSBr (0.473 and 0.0531 mmol, respectively) and stirred at rt overnight. The products were precipitated with DCM, filtered, washed with acetone and dried under reduced pressure.
Deprotected SiPcGal$_2$ MS (MALDI, DCTB+NaI) results were: m/z calculated for $C_{44}H_{38}N_8O_{12}Si$ $[M]^+$: 898.2, found: 574.2 (**SiPc(OH)$_2$**).
Deprotected SiPcGal$_4$ MS (MALDI, DCTB+NaI) results were: m/z calculated for $C_{68}H_{72}N_{14}O_{28}Si$ $[M]^+$: 1560.4, found: 574.2 (**SiPc(OH)$_2$**).

Part 2

Photophysical and photochemical studies of galacto-conjugates

2. Photophysical and photochemical studies of galacto-conjugates

2.1 Equipment and reagents

2.1.1 Equipment

The UV-visible assays were performed on the UVIKON 922 spectrophotometer from Biotek Instruments.

The illumination system used to determine the photostability of the PSs was the Light Source Model LC-122 from LumaCare, equipped with a halogen/quartz 250 W lamp coupled to one optic fiber probe (400-800 nm). The fluence rates were determined with the energy meter Coherent FieldMaxII-Top with a Coherent PowerSens PS19Q energy sensor.

For the $^1O_2$ generation study it was used a Light Emitting Diode (LED) array prepared by Mr. Cândido Casqueira, electromechanic technician of the Department of Chemistry of the University of Aveiro. It is composed of a matrix of 6 x 8 LEDs which makes a total of 48 light sources, emitting red light (λ > 600 nm). The regulated Plug-in adaptor with LED indicator 800 mA was purchased from Mean Well (MW).

2.1.2 Reagents, chemical products and buffers

SiPcGal$_4$, SiPcGal$_2$ and **SiPc(OH)$_2$** were synthesized as described in **Part 1**.

DMSO, DMF and DPBF were obtained from Fisher Scientific. PBS buffer was prepared in Milli-Q water at pH 7.60: 10 mM NaH_2PO_4, 70 mM Na_2HPO_4 and 145 mM NaCl.

2.1.3 Softwares

Microsoft Excel and GraphPad Prism 5.00 were used for the displayed graphs.

2.2 Experimental procedures

2.2.1 Aggregation assays

The aggregation behavior of the PSs in PBS buffer, DMSO and DMF was studied at different concentrations by Lambert-Beer´s law plots. This equation is based on the linear correlation between absorbance (A), molar absorptivity of the compound (ε, $L.mol^{-1}.cm^{-1}$), length of the light path (b, cm) and concentration of the compound in solution (c, mol.L-1) (121).

First, stock solutions of the galacto-conjugates (330 µM) were prepared in DMSO and frozen. The working solutions were freshly prepared by diluting the stock solutions in PBS buffer (1.25-10 µM) with the concentration of DMSO being always inferior to 3% (v/v). Quartz cuvettes holding one milliliter of working solutions (without air bubbles) were placed into the spectrophotometer and the absorbance was scanned for wavelengths between 300 to 800 nm. The wavelengths of maximum absorption were determined and the molar absorptivity of the compounds was calculated by plotting the absorbance against the respective concentration, by Lambert -Beer´s law, considering the length of the light path (b) equal to 1 cm. The same procedure was performed with the compounds dissolved in complete DMSO and DMF.

2.2.2 Fluorescence emission assay

SiPcGal$_4$, **SiPcGal$_2$** and **SiPc(OH)$_2$** working solutions were freshly prepared in DMF to give absorbance near 0.03 (conditions that minimize reabsorption of radiation by the ground-state species) at 601 nm. The fluorescence emission spectra of the PSs were measured between 620 to 800 nm, after excitation at 601 nm. The excitation and emission slits width were set at 2.0 nm.

2.2.3 Photostability assays

The photostability of PSs was determined by monitoring the decrease of the absorbance of Q bands, after different times of irradiation with red light (400-800 nm) delivered by an illumination system. Solutions of PSs at 20 µM were prepared in PBS buffer (6% v/v DMSO) and kept in the dark at rt. The study was performed in magnetically stirred cuvette solutions (with 1 mL of sample) in a dark room, over an irradiation time of 30 min with red light at a fluence rate of 150 mW.cm^{-2}. The absorbance between 640 and 730 nm (Q band that corresponds to the maximum absorbance of PSs) was determined before and after irradiation (1, 3, 4, 5, 10, 15, 20 and 30 min). After that, the photostability percentage was calculated with the following equation:

$$Photostability\ (\%) = \frac{Abs\ at\ a\ given\ time\ of\ irradiation}{Abs\ before\ irradiation}$$

2.2.4 Singlet oxygen assays

Singlet oxygen was determined through an indirect chemical method using DPBF as $^1O_2$ scavenger (122). The DPBF reacts specifically with $^1O_2$ in a [4+2] cycloaddition reaction, being oxidized to the colorless o-dibenzoylbenzene. Once DPBF has an absorption maximum at 415 nm, the ability of the PSs to generate $^1O_2$ is obtained by measuring the DPBF absorption decay, at this wavelength.

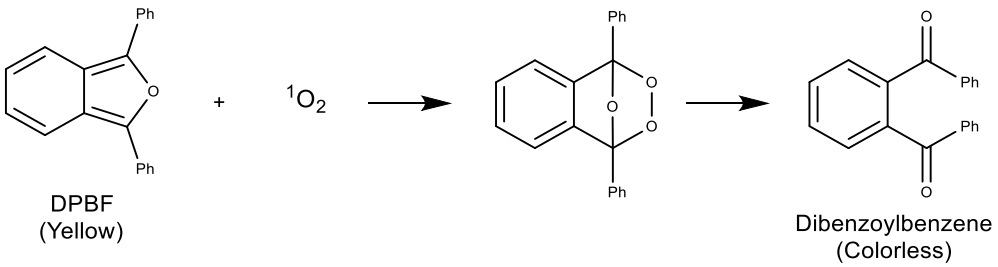

Scheme 4.1. Reaction of DPBF with $^1O_2$ by a Diels Alder reaction.

Solutions containing DPBF (30 µM) with or without the PSs (0.30 µM) were prepared in DMF in a one milliliter quartz cuvette. The solutions were irradiated at rt and under gentle magnetic stirring, with red light at a fluence rate of 5 $mW.cm^{-2}$. The decreasing of DPBF absorbance value at 415 nm was monitored at pre-established irradiation intervals. The results were expressed by plotting the DPBF depletion against the irradiation time. The depletion of DPBF was calculated according to the following equation:

$$DPBF\ depletion = \frac{Abs_t}{Abs_0}$$

Abs_0 and Abs_t are the absorbance values at 415 nm before and after irradiation, respectively.

Part 3

In vitro biological studies

3. *In vitro* biological studies

3.1 Equipment, materials and reagents

3.1.1 Equipment

The centrifuge used was a SIGMA 2-16 and the microcentrifuge was a VWR MiniFuge Galaxy MiniStar C1413. The vortex was from VWR. The liquid aspirator system used was the Vacusip from Integra. The shaker used was a standard analog shaker from VWR.

The UV-visible absorbance measurements were performed on a microplate reader Synergy™ HT (Biotek Instruments) controlled by BioTek's Gen5™ Data Analysis Software. The fluorescence measurements were determined using the Typhoon FLA 9000 in combination with its Image Quant TL software.

Photodynamic irradiation was carried out with red light (620-750 nm) delivered by an illumination system (LC-122 LumaCare, London). The light was delivered for 40 min at a fluence rate of 2.5 mW/cm^2, as measured with an energy meter (Coherent FieldMaxII-Top) combined with a Coherent PowerSens PS19Q energy sensor.

The fluorescence microscope was purchased from Leica DFC350 FX, Leica Microsystems, Bannockburn, IL, USA.

3.1.2 Materials

Canted neck cell culture flasks 75 cm^2 with 0.2 µM vent cap were purchased from Corning. CyroPure tubes were purchased from SARSTEDT. The tissue culture test plates and the conical tubes of 15 mL or 50 mL were from Orange Scientific. The Neubauer chamber was from VWR. The plates used were transparent (Orange Scientific) and black (Greiner Bio -One) 96-wells microtiter plates for the absorbance and fluorescence studies, respectively.

3.1.3 Cell culture/trypsin/kit/probes

UM-UC-3 (ATCC® Number: CRL-1749™), human bladder transitional carcinoma cell line, have been isolated from urinary bladder of a male caucasian.

Roswell Park Memorial Institute (RPMI)-4130 medium (Sigma) supplemented with 2 $g \cdot L^{-1}$ sodium bicarbonate (Sigma), 2 mM L-glutamine (Sigma), 10% (v/v) of heat-inactivated Fetal Bovine Serum (FBS; Life Technologies, Carlsbad, CA, USA) and antibiotic/antimycotic containing 100 $units \cdot mL^{-1}$ penicillin, 100 $\mu g \cdot mL^{-1}$ streptomycin and 0.25 $\mu g \cdot mL^{-1}$ amphotericin B (Sigma).

Trypsin Tryple Express was purchased from Gibco (Ref. 12605-010).

The Pierce BCA Protein Assay Kit-Reducing Agent Compatible (containing the BCA Protein Assay Reagent and bovine serum albumin (BSA) standards at 2 $mg.mL^{-1}$) was purchased from Thermo Scientific.

The 4′,6-Diamidino-2-phenylindole (DAPI) was purchased from Enzo Life Sciences. The H_2DCFDA (2',7'-dichlorohydrofluorescin) and DHE (dihydroethidium) were purchased from Life Sciences. MiyoPy1 (Mitochondria peroxy yellow 1) was obtained by Sigma-Aldrich.

3.1.4 Reagents, chemical products and buffers

$SiPcGal_4$, $SiPcGal_2$ and **$SiPc(OH)_2$** were synthesized as described in **Part 1**.

Paraformaldehyde (PFA) was from Merck and sodium dodecyl sulfate (SDS) and 3-[4,5-dimethylthiazol-2-yl]-2,5-diphenyltetrazolium bromide (MTT) were purchased from Sigma-Aldrich.

The trypan blue stain 0.4% was from BioWhittaker Reagents, Lonza. The hydrochloric acid (HCl) 37% was from Panreac.

The VectaSHIELD mounting medium with DAPI was purchased from VECTOR.

PBS buffer is composed of 137 mM NaCl, 27 mM KCl, 81 mM Na_2HPO_4, 15 mM KH_2PO_4 and is prepared in Milli-Q water. 1% SDS lysis buffer has 1% (v/v) SDS.

3.1.5 Softwares

Paint Shop Pro™ (v.6.00, Jasc Software) was used for the treatment of the images obtained in microscopy. GraphPad Prism (v.5.00, GraphPad Software) was used for most of the displayed graphs, as well as for the statistical analysis.

3.1.6 Statistical Analysis

The results are presented as mean ± standard error of the mean (S.E.M.) with *n* indicating the number of experiments. Statistical significance among two conditions was assessed using the nonparametric Mann-Whitney test. Statistical significance among three conditions was assessed by the nonparametric Kruskal-Wallis test. Statistical significance among several conditions was assessed with the Friedman test. P-value was considered at the 5% level of significance to deduce inference of the significance of the data.

3.2 Experimental procedures

3.2.1 Cell culture and subculture

UM-UC-3 cells were grown in RPMI medium. After two to three days, confluent cells were subcultured. The medium was removed from culture flasks by aspiration and discarded. The cell layers were washed with 10 mL of pre-warmed sterile PBS, in order to remove traces of FBS that would inhibit the action of the trypsin. After that, the cells were treated with 2.5 mL of trypsin Tryple Express and incubated during 5 min at 37 ºC until the cells rounded up and the cell layer start to disperse. The trypsinization progress was monitored under an inverted microscope. After incubation, RPMI medium was added to inhibit further tryptic activity and the cells were dispersed by repeated pippeting over the monolayer surface. The cells suspensions were then centrifuged at 1,000 *x g* for 5 min. The supernatant was removed, the cells were re-suspended in RPMI medium and appropriate aliquots of cells were added to new 75 cm^2 culture flasks. Cells were examined carefully every

day by eye on an inverted microscope, for signs of contamination and the RPMI medium was changed two or three times per week (118).

3.2.2 Preparation and treatment of UM-UC-3 cells with photosensitizers

After the removal of supernatant and the re-suspension of the cells in 10 mL of RPMI medium as described before, 20 µL of cell suspension was mixed with 20 µL of trypan blue stain to determine cellular viability. Trypan Blue is an organic amine dye that is excluded by living cells with intact membranes, while death cells, where the plasma membrane integrity is compromised, take up the dye. Thus, all the cells that are blushed with the dye are considered non-viable and appear with a blue color in the microscope. On the other hand, viable cells will appear brilliant. Cells were counted using a haemocytometer. The percentage of viable cells and the concentration of cells per milliliter of cell suspension were calculated according to the following equations:

$$Viable\ cells\ (\%) = \frac{Nº\ of\ viable\ cells}{Nº\ \ of\ total\ cells} \times 100$$

$$\frac{Viable\ cells}{mL} = \frac{VCs\ \times dilution\ factor}{1 \times 10^{-4}}$$

Only cells with viability superior to 90% were utilized in the experiments. The viable cells concentration was calculated considering the average of viable cells (VCs) per each counting square, the dilution made and the volume of each counting square.

After this, UM-UC-3 cells were seeded into cell culture plates of 24 or 96-wells according to the experiment, at a density of 18 x 10^4 and 3 x 10^4 cells.cm^{-2} respectively, and incubated overnight in an incubator at 37 ºC with 5% CO_2 and 95% air to promote cell adhesion. On the following day, the UM-UC-3 cells growing in monolayer culture were treated with desired concentrations of sterile solutions of PSs.

Stock solutions of the PSs at a concentration of 330 µM were prepared in sterile DMSO and stored at 0-4 ºC in dark conditions. Freshly working solutions with different concentrations were obtained from the respective stock solution in sterile PBS, accounting their water solubility range. The concentration of DMSO was always lower than 0.5% (v/v), in all working solutions.

3.2.3 Determination of intracellular PS concentration by fluorimetry

Taking into account the fluorescence properties of the Pcs, their concentration inside the cancer cells can be determined by fluorimetry (after cell lysis) and normalized to total protein quantity. The protein quantification was measured spectrophotometrically using the Bicinchoninic Acid Assay (BCA assay), also known as the Smith assay (123). The procedure involves two fundamental steps: 1) biuret reaction, where the cupric ion (Cu^{2+}) is reduced to cuprous ion (Cu^{+}) by peptide bonds in proteins, in an alkaline environment, resulting in a blue color, and therefore, the amount of reduced Cu^{2+} is proportional to the amount of protein present in the solution; 2) the chelation of two molecules of BCA with one cuprous ion results in an intense purple-colored product that can be measure at any wavelength between 550 nm and 570 nm.

A. Determination of intracellular PS fluorescence

UM-UC-3 cells were seeded into 96-wells cell culture plates at a density of 3 x 10^4 cells per well (final volume of 100 µL per well) and incubated overnight in an incubator at 37 ºC with 5% CO_2 and 95% air. On the following day, immediately after PSs incubation, cells were washed twice with PBS. Then, they were mechanically scrapped in 120 µL of 1% (m/v) SDS solution in PBS (pH 7.0) and the plate was stirred on an automatic plate shaker in the dark at rt. 90 µL of this cell suspension were transferred to 96-wells black plates and the intracellular fluorescence of the PSs was determined by fluorometric measurement, using standard PSs solutions (0 – 6.25 µM) for calibration (**Figure 4.1**). The intracellular fluorescence was determined using a Typhoon FLA 9000 imager (GE Healthcare) with a 100-µm spot

resolution and 300 V. The excitation and emission wavelengths were set at 635 nm (red LD laser) and LPR (665LP), respectively. The PS concentration in the samples was directly obtained by plotting the average of the fluorescence for each PS standard in function of its concentration (µM). The results were normalized for protein concentration.

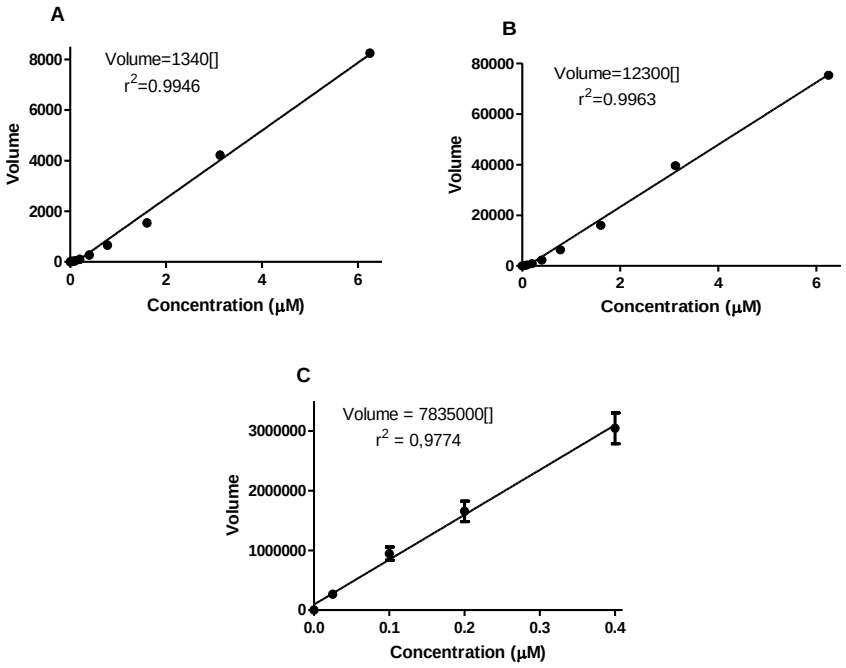

Figure 4.1 Calibration slopes of the PSs (**$SiPcGal_4$** (**A**)**, $SiPcGal_2$** (**B**) and **$SiPc(OH)_2$** (**C**)) fluorescence average in function of their standard concentrations (0 - 6.25 µM).

B. Determination of protein concentration

In a 96-wells plate, the following solutions were pipetted into each well:

- 25 µL of sample buffer: 1% (m/v) SDS in PBS (pH 7.0),

- 25 µL of sample, blank (sample buffer), standard (prepared in the sample buffer at concentrations ranging from 12.5-800 $\mu g.mL^{-1}$ using the BSA standard at 2 $mg.mL^{-1}$),

- 150 µL of BCA working Reagent (50 parts of BCA reagent A mixed with one part of BCA reagent B).

The plate was incubated at 37 ºC for 30 min. Then, the absorbance at 570 nm was measured in the plate reader spectrophotometer. The protein concentration

in the samples was directly obtained by plotting the average of the absorbance at 570 nm for each BSA standard in function of its concentration (µg.mL^{-1}).

3.2.4 Determination of intracellular PS fluorescence by fluorescence microscopy

Knowing the fluorescence properties of Pcs, their intracellular fluorescence can also be evaluated by fluorescence microscopy. Coverslips (one per well in 24-wells culture plates) were coated with poly-L-lysine for 1 h at rt. Then, after drying completely the UM-UC-3 were plated at a density of 18 x 10^4 cells per well (200 µL per well), in 24-wells culture plates for 3 h before treatment. After PS uptake and washing, cells were fixed with 4% PFA for 10 min at rt. The samples were washed with PBS (2 x 5 min). The coverslips were mounted using Vectashield sealed with nail polish and stored at 4 ºC until visualization under the fluorescence microscope.

3.2.5 Photodynamic Assays

The desired effect that is expected to obtain after photo-activation of PS is not only its preferential accumulation in cancer cells, but also its toxicity only upon light irradiation. That is why it is important to study the PSs toxicity in the absence and presence of light irradiation.

After PSs incubation, cells were washed with PBS and then it was added 100 µL of RPMI medium to cover the cells. In a dark room, cells were irradiated during 40 min with red light at a potency of 2.5 mW.cm^{-2}. After irradiation, cells were incubated in the humidified incubator gassed with 5% CO_2 and 95% air.

3.2.6 Cell viability assay

To evaluate the toxicity and phototoxicity of the PSs the MTT assay was used. In living cells, MTT is reduced by the mitochondrial enzyme succinate dehydrogenase to the insoluble blue purple formazan crystals, which means that it

is possible to correlate the reduction of MTT with this enzyme activity and therefore with the cellular viability (124).

UM-UC-3 cells were plated before at a density of 3 x 10^4 cells per well, in 96-wells culture plates for 24 h before treatment and then were treated with the PSs. The photodynamic treatment was performed and after 24 h, 50 µL of the medium was removed and 10 µL of MTT stock solution (3 $mg.mL^{-1}$ in PBS buffer) was added to each well in order to obtain a final concentration of 0.5 $mg.mL^{-1}$. The plates were then incubated at 37 ºC with 5% CO_2 and 95% air for 3 h. After that, the formed purple crystals were dissolved by the addition of 150 µL of acidic isopropanol (0.04 M HCl in absolute isopropanol), with repeated pipetting. The absorbance was measured at 570 nm (using 620 nm as the background wavelength), using a plate reader spectrophotometer: Absorbance 570 nm – Absorbance 620 nm. The percentage of absorbance for each treated sample was normalized to each untreated control cells (cells incubated with only PBS):

$$MTT\ reduction\ (\%) = \frac{Abs\ (treated\ samples)}{Abs\ (untreated\ samples)} \times 100$$

3.2.7 Intracellular levels of Reactive Oxygen Species after PDT

The ROS generation after PDT were detected using three different probes: H_2DCFDA (118), DHE (119) and MitoPy1 (120), by fluorescence spectroscopy technique. H_2DCFDA is able to cross the cell membrane and intracellular esterases remove its acetate groups, producing H_2DCF that will react with several cytotoxic ROS and form DCF which fluorescence intensity can be measured and be directly correlated with the intracellular ROS levels. DHE probe has blue fluorescence and it diffuses across cell membrane. $O_2^{\bullet -}$ anions oxidize DHE to ethidium, which intercalates within the cell's DNA, staining the nucleus with bright red fluorescence. MitoPy1 probe selectively tracks to the mitochondria and responds to local fluxes of H_2O_2 with a turn-on fluorescence increase.

UM-UC-3 cells were plated in 96-wells black plates for 24 h before treatment. After photodynamic treatment and washing, cells were incubated with 5 µM of the

three probes, under dark conditions, for 1 h at 37ºC. After incubation, cells were washed with PBS and mechanically scrapped in 1% (m/v) SDS solution in PBS (pH 7.0). Then, the intracellular fluorescence was measured with excitation and emission filters of 485/20 and 590/35 nm for H_2DCFDA, 485/20 and 528/20 nm for DHE and MitoPy1. Protein concentration was determined using the Pierce® BCA Protein Assay Kit as described previously.

CHAPTER V

BIBLIOGRAPHY

v. Bibliography

1. Stewart BW, Wild CP. World Cancer Report 2014. 1 ed. Lyon: International Agency for Research on Cancer; 2014.

2. Zheng X, Pandey RK. Porphyrin-Carbohydrate Conjugates: Impact of Carbohydrate Moieties in Photodynamic Therapy (PDT). *Anti Cancer agents MedChem*. 2008; 8: p. 241–68.

3. Agostinis P, Berg K, Cengel KA, Foster TH, Girotti AW, Gollnick SO. Photodynamic Therapy of Cancer: An Update. *CA-Cancer J Clin*. 2011; 61: p. 250–81.

4. David A. Carbohydrate-based Biomedical Copolymers for Targeted Delivery of Anticancer Drugs. *Isr J Chem*. 2010; 50: p. 204–19.

5. Tanaka M, Kataoka H, Yano S, Ohi H, Moriwaki K, Akashi H. Antitumor effects in gastrointestinal stromal tumors using photodynamic therapy with a novel glucose-conjugated chlorin. *Mol Cancer Ther.* 2014; 13: p. 767–75.

6. Tanaka T, Matono S, Nagano T, Murata K. Photodynamic therapy for large superficial squamous cell carcinoma of the esophagus. *Gastroinstest Endosc*.; 2011; 73: p. 1–6.

7. Tanaka M, Kinoshita M, Yoshihara Y. Photodynamic Therapy Using Intra-Articular Photofrin for Murine MRSA Arthritis: Biphasic Light Dose Response for Neutrophil-Mediated Antibacterial Effect. *Lasers Surg Med*. 2011; 43: p. 221–9.

8. Dolmans DEJGJ, Kadambi A, Hill JS, Waters CA, Robinson BC, Walker JP. Vascular Accumulation of a Novel Photosensitizer, MV6401, Causes Selective Thrombosis in Tumor Vessels after Photodynamic Therapy 1. *Cancer Res*. 2002; 62: p. 2151–6.

9. Von Tappeiner H and Jesionek H. Therapeutische versuche mit fluoreszierenden stoffen. *Munch Med Wochenschr*. 1903; 47: p. 2042–4.

10. MEYER-BETZ F. Untersuchungen über die biologische (photodynamische) Wirkung des Hämatoporphyrins und anderer Derivate des Blut- und Gallenfarbstoffs. *Arch Klin Med*. 1913; 112: p. 476–503.

11. Schwartz S, Absolon K, Vermund H. Effect of porphyrins on x-ray sensitivity of tumors. *J Lab Clin Med*. 1955; 46: p. 949.

12. Dolmans DEJGJ, Fukumura D, Jain RK. Photodynamic therapy for cancer. *Nat Rev Cancer*. 2003; 3: p. 380–7.

13. Sessler JL, Hemmi G, Mody TD, Murai T, Burrell A, Young SW. Texaphyrins: Synthesis and Applications. *Acc Chem Res*. 1994; 27: p. 43–50.

14. Mellish KJ, Brown SB. Verteporfin: a milestone in opthalmology and photodynamic therapy. *Expert Opinion on Pharmacotherapy*. 2001; 2: p. 351-61.

15. Singh S, Aggarwal A, Thompson S, Tome PC, Zhu X, Samaroo D. Synthesis and Photophysical Properties of Thioglycosylated Chlorins, Isobacteriochlorins, and Bacteriochlorins for Bioimaging and Diagnostics. *Bioconjugate Chem*. 2010; 21: p. 2136–46.

16. Lourenço LMO, Neves MGPMS, Cavaleiro JAS, Tomé JPC. Synthetic approaches to glycophthalocyanines. *Tetrahedron*. 2014; 70: p. 2681–98.

17. Nishiyama N, Morimoto Y, Jang W-D, Kataoka K. Design and development of dendrimer photosensitizer-incorporated polymeric micelles for enhanced photodynamic therapy. *Adv Drug Deliv Rev*. 2009; 61: p. 327–38.

18. Juarranz Á, Jaén P, Sanz-Rodríguez F, Cuevas J, González S. Photodynamic therapy of cancer. Basic principles and applications. *Clin Transl Oncol*. 2008; 10: p. 148–54.

19. Castano AP, Demidova TN, Hamblin MR. Mechanisms in photodynamic therapy: part one—photosensitizers, photochemistry and cellular localization. *Photodiagnosis Photodyn Ther*. 2004; 1: p. 279–93.

20. Henderson W, Dougherty J. How does photodynamic therapy work? *Photochem Photociol.*1992; 55: p. 145–57.

21. Gorman a. a., Lovering G, Rodgers MAJ. A pulse radiolysis study of the triplet sensitized production of singlet oxygen: determination of energy transfer efficiencies. *J Am Chem Soc*. 1978; 100: p. 4527–32.

22. Josefsen LB, Boyle RW. Unique diagnostic and therapeutic roles of porphyrins and phthalocyanines in photodynamic therapy, imaging and theranostics. *Theranostics*. 2012; 2: p. 916–66.

23. Dougherty TJ, Cooper MT, Mang TS. Cutaneous phototoxic occurrences in patients receiving Photofrin®. *Lasers Surg Med*. 1990; 10: p. 485–8.

24. Roberts SA. Drug metabolism and pharmacokinetics in drug discovery. *Curr Opin Drug Discov Devel*. 2003; 6: p. 66–80.

25. Kola I, Landis J. Can the pharmaceutical industry reduce attrition rates? *Nat Rev Drug Discov*. 2004; 3: p. 711–5.

26. Balani SK, Miwa GT, Gan L-S, Wu J-T, Lee FW. Strategy of utilizing *in vitro* and *in vivo* ADME tools for lead optimization and drug candidate selection. *Curr Top Med Chem*. 2005; 5: p. 1033–8.

27. Goodman & Gilman. The Pharmacological Basis of Therapeutics. 11 ed. California: McGraw-Hill companies; 2006.

28. Markovsky E, Baabur-Cohen H, Eldar-Boock A, Omer L, Tiram G, Ferber S. Administration, distribution, metabolism and elimination of polymer therapeutics. *J Control Release*. 2012; 161: p. 446–60.

29. Dougherty TJ, inventor; Health Research Inc., assignee. Photodynamic therapy with *in situ* activation of photosensitiser - by reaction of components separately encapsulated in liposomes which melt when the tumour is heated by microwave, laser, etc. United States patent US 5257970-A. 1993 Nov 2.

30. Wi D, Hirth A, Bogdahn-rai T, Schnurpfeil G, Shopova M. Photodynamic therapy of cancer : second and third generations of photosensitizers. *Russ Chem B*+. 1998; 47: p. 836–45.

31. Kennedy J. Photodynamic therapy with endogenous protoporphyrin ix : basic principles and present clinical experience. *J Photochem Photobiol*. 1990; 6: p. 143–8.

32. Jichlinski P, Jacqmin D. Photodynamic Diagnosis in Non-Muscle-Invasive Bladder Cancer. *Eur Urol Suppl*. 2008; 7: p. 529–35.

33. Pereira PMR, Carvalho JJ, Silva S, Cavaleiro J a S, Schneider RJ, Fernandes R. Porphyrin conjugated with serum albumins and monoclonal antibodies boosts efficiency in targeted destruction of human bladder cancer cells. *Org Biomol Chem*. 2014; 12: p. 1804–11.

34. Mitsunaga M, Ogawa M, Kosaka N, Rosenblum LT, Choyke PL, Kobayashi H. Cancer cell-selective *in vivo* near infrared photoimmunotherapy targeting specific membrane molecules. *Nat Med*. 2011; 17: p. 1685–91.

35. Serra VV, Zamarrón A, Faustino MAF, Iglesias-de la Cruz MC, Blázquez A, Rodrigues JMM. New porphyrin amino acid conjugates: synthesis and photodynamic effect in human epithelial cells. *Bioorg Med Chem*. 2010; 18: p. 6170–8.

36. Ernst B, Magnani JL. From carbohydrate leads to glycomimetic drugs. *Nat Rev Drug Discov*. 2009; 8: p. 661–77.

37. Figueira F, Pereira PMR, Silva S, Cavaleiro JAS, Tomé JPC. Porphyrins and Phthalocyanines Decorated with Dendrimers : Synthesis and Biomedical Applications. *Curr Org Chem*. 2014; 11: p. 110–26.

38. Tomé JPC, Neves MGPMS, Tomé AC, Cavaleiro JAS, Mendonça AF, Pegado IN. Synthesis of glycoporphyrin derivatives and their antiviral activity against herpes simplex virus types 1 and 2. *Bioorg Med Chem*. 2005; 13: p. 3878–88.

39. Lourenço LMO, Tomé JPC, Domingues MRM, Domingues P, Costa PJ, Félix V. Synthesis and differentiation of alpha- and beta-glycoporphyrin stereoisomers by electrospray tandem mass spectrometry. *Rapid Commun Mass Spectrom*. 2009; 23: p. 3478–83.

40. Pereira PMR, Silva S, Cavaleiro J a S, Ribeiro C a F, Tomé JPC, Fernandes R. Galactodendritic phthalocyanine targets carbohydrate-binding proteins enhancing photodynamic therapy. *PLoS One*. 2014; 9: p. e95529.

41. Tarragó-Trani MT, Jiang S, Harich KC, Storrie B. Shiga-like toxin subunit B (SLTB)-enhanced delivery of chlorin e6 (Ce6) improves cell killing. *Photochem Photobiol*. 2006; 82: p. 527–37.

42. Maillard P, Hery C, Momenteau M. Synthesis, characterization and photocytotoxicity of a glycoconjugated meso-monoarylbenzochlorin. *Tetrahedron Lett*. 1997; 38: p. 3731–4.

43. Fujimoto K, Miyata T, Aoyama Y. Saccharide-Directed Cell Recognition and Molecular Delivery Using Macrocyclic Saccharide Clusters: Masking of Hydrophobicity to Enhance the Saccharide Specificity. *J Am Chem Soc*. 2000; 122: p. 3558–9.

44. Tanaka M, Kataoka H, Mabuchi M, Sakuma S, Takahashi S, Tujii R. Anticancer effects of novel photodynamic therapy with glycoconjugated chlorin for gastric and colon cancer. *Anticancer Res*. 2011; 31: p. 763–9.

45. Lee PPS, Lo PC, Chan EYM, Fong WP, Ko WH, Ng DKP. Synthesis and *in vitro* photodynamic activity of novel galactose-containing phthalocyanines. *Tetrahedron Lett*. 2005; 46: p. 1551–4.

46. De la Torre G, Bottari G, Hahn U, Torres T. Functional Phthalocyanines: Synthesis, Nanostructuration, and Electro-Optical Applications. In: Jiang J, editor. Functional Phthalocyanine Molecular Materials. 1 ed. Berlin, Heidelberg: Springer; 2010. p. 1-44.

47. Van Leeuwen M, Beeby A, Fernandes I, Ashworth SH. The photochemistry and photophysics of a series of alpha octa(alkyl-substituted) silicon, zinc and palladium phthalocyanines. *Photochem Photobiol Sci*. 2014; 13: p. 62–9.

48. Lier JE Van, Spikest JD. The chemistry , photophysics and photosensitizing properties of phthalocyanines. *Novartis Found Symp*. 1989; 146: p. 17–39.

49. Garland MJ, Cassidy CM, Woolfson D, Donnelly RF. Designing photosensitizers for photodynamic therapy: strategies, challenges and promising developments. *Future Med Chem*. 2009; 1: p. 667–91.

50. McKeown NB. Phthalocyanines: Synthesis. In: Kadish, K. M.; Smith, K. M.; Guilard R, editors. The Porphyrin Handbook. 1 ed. New York: Academic Press Inc; 2003. p. 177-246.

51. Doane T, Chomas A, Srinivasan S, Burda C. Observation and photophysical characterization of silicon phthalocyanine J-aggregate dimers in aqueous solutions. *Chem Eur J*. 2014; 20: p. 8030–9.

52. Luan L, Ding L, Shi J, Fang W, Ni Y, Liu W. Effect of axial ligands on the molecular configurations, stability, reactivity, and photodynamic activities of silicon phthalocyanines. *Chem Asian J*. 2014; 9: p. 3491–7.

53. Oleinick NL, Antunez AR, Clay ME, Rihter BD, Kenney ME. New phthalocyanine photosensitizers for photodynamic therapy. *Photochem Photobiol*. 1993; 57: p. 242–7.

54. Zaidi SI, Oleinick NL, Zaim MT, Mukhtar H. Apoptosis during photodynamic therapy-induced ablation of RIF-1 tumors in C3H mice: electron microscopic,

histopathologic and biochemical evidence. *Photochem Photobiol*. 1993; 58: p. 771–6.

55. Swick A, Camouse M, McCormick T. Successful penetration of topically-applied silicon phthalocyanine photosensitizer Pc 4 and new Pc 4 salts into human skin. *J Invest Dermatol*. 2004; 122: p. A146–A146.

56. Baron ED, Malbasa CL, Santo-Domingo D, Fu P, Miller JD, Hanneman KK. Silicon phthalocyanine (Pc 4) photodynamic therapy is a safe modality for cutaneous neoplasms: results of a phase 1 clinical trial. *Lasers Surg Med*. 2010; 42: p. 728–35.

57. Doane TL, Chuang C-H, Chomas A, Burda C. Photophysics of silicon phthalocyanines in aqueous media. *Chem Phys Chem*. 2013; 14: p. 321–30.

58. Ben-Hur E, Oetjen J, Horowitz B. Silicon phthalocyanine Pc 4 and red light causes apoptosis in HIV-infected cells. *Photochem Photobiol*. 1997; 65: p. 456–60.

59. Huang J-D, Fong W-P, Chan EYM, Choi MTM, Chan W-K, Chan M-C. Photodynamic activities of a dicationic silicon(IV) phthalocyanine and its bovine serum albumin conjugates. *Tetrahedron Lett*. 2003; 44: p. 8029–32.

60. Jiang XJ, Huang JD, Zhu YJ, Tang FX, Ng DKP, Sun JC. Preparation and *in vitro* photodynamic activities of novel axially substituted silicon (IV) phthalocyanines and their bovine serum albumin conjugates. *Bioorganic Med Chem Lett*. 2006; 16: p. 2450–3.

61. Shen X-M, Zheng B-Y, Huang X-R, Wang L, Huang J-D. The first silicon(IV) phthalocyanine-nucleoside conjugates with high photodynamic activity. *Dalton Trans*. 2013; 42: p. 10398–403.

62. Lau JTF, Lo P-C, Tsang Y-M, Fong W-P, Ng DKP. Unsymmetrical β-cyclodextrin-conjugated silicon(IV) phthalocyanines as highly potent photosensitisers for photodynamic therapy. *Chem Commun (Camb)*. 2011; 47: p. 9657–9.

63. Lo PC, Chan CMH, Liu JY, Fong WP, Ng DKP. Highly photocytotoxic glucosylated silicon(IV) phthalocyanines. Effects of peripheral chloro substitution on the photophysical and photodynamic properties. *J Med Chem*. 2007; 50: p. 2100–7.

64. Lo P-C, Leung SCH, Chan EYM, Fong W-P, Ko W-H, Ng DKP. Photodynamic effects of a novel series of silicon(IV) phthalocyanines against human colon adenocarcinoma cells. *Photodiagnosis Photodyn Ther*. 2007; 4: p. 117–23.

65. Gabius H-J, André S, Jiménez-Barbero J, Romero A, Solís D. From lectin structure to functional glycomics: principles of the sugar code. *Trends Biochem Sci*. 2011; 36: p. 298–313.

66. Sharon N, Lis H. Lectins as cell recognition molecules. *Science (80-)*. 1989; 246: p. 227–34.

67. Liu F-T, Rabinovich G a. Galectins as modulators of tumour progression. *Nat Rev Cancer*. 2005; 5: p. 29–41.

68. Indolo LC, Envenuto GB, Alvatore PS, Ero RP, Alvatore GS, Irone VM. Galectin-1 and galectin-3 expression in human bladder transitional-cell carcinomas. 1999; 43: p. 39–43.

69. D'Auria S, Petrova L, John C, Russev G, Varriale A, Bogoeva V. Tumor-specific protein human galectin-1 interacts with anticancer agents. *Mol Biosyst*. 2009; 5: p. 1331–6.

70. Yang R-Y, Rabinovich G a, Liu F-T. Galectins: structure, function and therapeutic potential. *Expert Rev Mol Med*. 2008; 10: p. e17.

71. Liu F-T, Rabinovich GA. Galectins as modulators of tumour progression. *Nat Rev Cancer*. 2005; 5: p. 29–41.

72. Silva S, Pereira PMR, Silva P, Paz FAA, Faustino MAF, Cavaleiro JAS. Porphyrin and phthalocyanine glycodendritic conjugates: synthesis, photophysical and photochemical properties. *Chem Commun (Camb)*. 2012; 48: p. 3608–10.

73. Gillies ER, Fréchet JMJ. Dendrimers and dendritic polymers in drug delivery well as agents for both boron neutron capture therapy and photodynamic therapy. *Drug Discovery Today*. 2005; 10. p. 35-43.

74. Brown SB, Brown EA, Walker I. The present and future role of photodynamic therapy in cancer treatment. *Lancet Oncol*. 2004; 5: p. 497–508.

75. Macdonald IJ, Dougherty TJ. Basic principles of photodynamic therapy. *JPP*. 2001; 5: p. 105–29.

76. Pereira PMR. Conjugados fotoativos para o tratamento do cancro da bexiga [dissertação]. Aveiro: Universidade de Aveiro; 2012.

77. Kessel D, Erickson C. Porphyrin photosensitization of multi-drug resistant cell types. *Photochem Photobiol*. 1992; 55: p. 397–9.

78. Ploeg M, Aben KKH, Kiemeney LA. The present and future burden of urinary bladder cancer in the world. *World J Urol*. 2009; 27: p. 289–93.

79. Bassi P, Pagano F. Invasive Bladder Cancer. 1 ed. London: Springer; 2007.

80. Cheryl T. Lee DPW. Bladder Cancer - Diagnosis Therapeutics, and Management. 1 ed. New York: Humana Press; 2010.

81. Stephen BE, David RB, Carolyn CC, April G. AJCC Cancer Staging Manual. 7 ed. New York: Springer; 2009.

82. Geoffrey D. Chisholm. Clinical Practice in Urology. 1 ed. Berlin Heidelberg: Springer; 1985.

83. Urology Care Foundation. Bladder cancer [Web page] Linthicum: American Urological Association. 2011 [updated 2015; cited 2014 Dec 13]. Available from: http://www.urologyhealth.org/urology/index.cfm?article=100.

84. Fuessel S, Kunze D, Wirth MP. Bladder Cancer Biology. In: Abdullah Canda. Bladder Cancer - From Basic Science to Robotic Surgery. Rijeka: InTech; 2012 [cited 2015 29 Set]. Available from: http://www.intechopen.com/books/bladder-cancer-from-basic-science-to-robotic-surgery/bladder-cancer-biology

85. Ferlay J, Steliarova-Foucher E, Lortet-Tieulent J, Rosso S, Coebergh JWW, Comber H. Cancer incidence and mortality patterns in Europe: estimates for 40 countries in 2012. *Eur J Cancer*. 2013; 49: p. 1374–403.

86. Samaras V, Rafailidis PI, Mourtzoukou EG, Peppas G, Falagas ME. Chronic bacterial and parasitic infections and cancer: A review. *J. Infect. Dev. Ctries.* 2010. p. 267–81.

87. Robbins and Cotran. Pathologic Basis Of Disease. 7 ed. St Louis: Elsevier Saunders; 2005.

88. Seth P Lerner MPS and CNS. Treatment and Management of Bladder Cancer. 1 ed. London: Informa UK Ltd; 2008.

89. Morales A, Eidinger D, Bruce AW. Intracavitary Bacillus Calmette-Guerin in the treatment of superficial bladder tumors. *J Urol*. 1976; 116: p. 180–3.

90. Palou Redorta J. Management of BCG “Failures.” *Eur Urol*. 2006; 49: p. 779–80.

91. Goh AC, Lerner SP. Application of new technology in bladder cancer diagnosis and treatment. *World J Urol*. 2009; 27: p. 301–7.

92. Blandy J and Kaisary A. Urology. 6 ed. New Jersey: John Wiley & Sons; 2009.

93. Lourenço LMO, Pereira PMR, Maciel E, Válega M, Domingues FMJ, Domingues MRM. Amphiphilic phthalocyanine-cyclodextrin conjugates for cancer photodynamic therapy. *Chem Comm*. 2014; 50: p. 8363–6.

94. Kelly JF, Snell ME, Berenbaum MC. Photodynamic destruction of human bladder carcinoma. *Br J Cancer*. 1975; 31: p. 237–44.

95. Rosenberg SJ, Williams RD. Photodynamic therapy of bladder carcinoma. *Urol Clin North Am*. 1986; 13: p. 435–44.

96. Morales A. Treatment of superficial bladder cancer. *Can Med Assoc J*. 1980; 122: p. 1133–8.

97. Nseyo UO, Merrill DC, Lundahl SL. Green light photodynamic therapy in the human bladder. *Clin Laser Mon*. 1993; 11: p. 247–50.

98. Berger AP, Steiner H, Stenzl A, Akkad T, Bartsch G, Holtl L. Photodynamic therapy with intravesical instillation of 5-aminolevulinic acid for patients with recurrent superficial bladder cancer: A single-center study. *Urology*. 2003; 61: p. 338–41.

99. Baumgartner R, Waidelich R, Beyer W, Stepp HG, Knuechel-Clarke R, Hofstetter A, editors. Integral photodynamic therapy of bladder cancer using 5-ALA and white light: Proceedings of Photonic Therapeutics and Diagnostics conference; 2005 May 5; Bellingham: SPIE - The International Society for Optical Engineering; 2005.

100. Waidelich R, Beyer W, Knüchel R, Stepp H, Baumgartner R, Schröder J. Whole bladder photodynamic therapy with 5-aminolevulinic acid using a white light source. *Urology*. 2003; 61: p. 332–7.

101. Skyrme RJ, French AJ, Datta SN, Allman R, Mason MD, Matthews PN. A phase-1 study of sequential mitomycin C and 5-aminolaevulinic acid-mediated photodynamic therapy in recurrent superficial bladder carcinoma. *BJU Int*. 2005; 95: p. 1206–10.

102. Pan H, Ma X, Chen J, Jiang H. PDT combined with Intravesical BCG instillation would form an autovaccine for bladder cancer? *Med Hypotheses*. 2009; 73: p. 559–60.

103. Fabienne Dumoulin. Design and Conception of photosensitizers. In: Nyokong T**,** Ahsen V. Photosensitizers in Medicine, Environment, and Security. Dordrecht: Springer; 2012. p. 1-46.

104. Soares ARM, Tomé JPC, Neves MGPMS, Tomé AC, Cavaleiro JAS, Torres T. Synthesis of water-soluble phthalocyanines bearing four or eight d-galactose units. *Carbohydr Res*. 2009; 344: p. 507–10.

105. Carey FA. Organic chemistry. 4 ed. Virginia: McGraw Hill; 2011.

106. Van Poecke S, Barrett MO, Santhosh Kumar T, Sinnaeve D, Martins JC, Jacobson KA. Synthesis and $P2Y_2$ receptor agonist activities of uridine 5'-phosphonate analogues. *Bioorg Med Chem*. 2012; 20: p. 2304–15.

107. Masilela N, Antunes E, Nyokong T. Axial coordination of zinc and silicon phthalocyanines to silver and gold nanoparticles: an investigation of their photophysicochemical and antimicrobial behavior. *JPP*. 2013; 17: p. 417–30.

108. Leng X, Ng DKP. Axial Coordination of Porphyrinatocobalt (II) Complexes with Bis (pyridinolato) silicon (IV) Phthalocyanines. *Eur J Inorg Chem.* 2007; p. 4615–20.

109. Lo PC, Fong WP, Ng DKP. Effects of peripheral chloro substitution on the photophysical properties and *in vitro* photodynamic activities of galactose-conjugated silicon(IV) phthalocyanines. *Chem Med Chem*. 2008; 3: p. 1110–7.

110. Kim J, Santos OA, Park JH. Selective photosensitizer delivery into plasma membrane for effective photodynamic therapy. *J Control Release*. 2014; 191: p. 98–104.

111. Qiao X-F, Zhou J-C, Xiao J-W, Wang Y-F, Sun L-D, Yan C-H. Triple-functional core–shell structured upconversion luminescent nanoparticles covalently

grafted with photosensitizer for luminescent, magnetic resonance imaging and photodynamic therapy *in vitro*. *Nanoscale*. 2012; 4: p. 4611.

112. Leffler H, Nilsson UJ, Rudovica V. Synthesis of 1,2,3-triazole-linked galactohybrids and their inhibitory activities on galectins. *Arkivoc*. 2014; 2014: p. 90–112.

113. Lu J, Zhang W, Yuan L, Ma W, Li X, Lu W. One-pot synthesis of glycopolymer-porphyrin conjugate as photosensitizer for targeted cancer imaging and photodynamic therapy. *Macromol Biosci*. 2014; 14: p. 340–6.

114. Lv F, He X, Lu L, Wu L, Liu T. Synthesis, properties and near-infrared imaging evaluation of glucose conjugated zinc phthalocyanine via Click reaction. *JPP*. 2012; 16: p. 77–84.

115. Sorescu A, Nuta A, Raditoiu V, Ion R-M, editors. Photophysical and photochemical properties of some silicon benzporphyrazine derivatives: Proceedings of The 2nd year of ARSA - Advanced Research in Scientific Areas; 2013 Dez 2-6. EDIS - Publishing Institution of the University of Zilina; 2013.

116. Silva EMP, Ramos CIV, Pereira PMR, Giuntini F, Faustino MAF, Tomé JPC. Cationic β-vinyl substituted meso -tetraphenylporphyrins: synthesis and non-covalent interactions with a short poly(dGdC) duplex. *JPP*. 2012; 16: p. 101–13.

117. Baumgart E, Cohen MS, Silva Neto B, Jacobs M a, Wotkowicz C, Rieger-Christ KM. Identification and prognostic significance of an epithelial-mesenchymal transition expression profile in human bladder tumors. *Clin Cancer Res*. 2007; 13: p. 1685–94.

118. Chandel NS, Maltepe E, Goldwasser E, Mathieu CE, Simon MC, Schumacker PT. Mitochondrial reactive oxygen species trigger hypoxia-induced transcription. *Proc Natl Acad Sci USA*. 1998; 95: p. 11715–20.

119. Fernandes R, Hosoya K, Pereira P. Reactive oxygen species downregulate glucose transport system in retinal endothelial cells. *Am J Physiol Cell Physiol*. 2011; 300: p. C927–36.

120. Dickinson BC, Lin VS, Chang CJ. Preparation and use of MitoPY1 for imaging hydrogen peroxide in mitochondria of live cells. *Nat Protoc*. 2013; 8: p. 1249–59.

121. Swinehart F. The Beer-Lambert Law. *J Chem Educ.* 1962; 39: p. 333–5.

122. Oda K, Ogura SI, Okura I. Preparation of a water-soluble fluorinated zinc phthalocyanine and its effect for photodynamic therapy. *J Photochem Photobiol B Biol*. 2000; 59: p. 20–5.

123. Smith PK, Krohn RI, Hermanson GT, Mallia AK, Gartner FH, Provenzano MD. Measurement of protein using bicinchoninic acid. *Anal Biochem*. 1985; 150: p. 76–85.

124. Mosmann T. Rapid colorimetric assay for cellular growth and survival: Application to proliferation and cytotoxicity assays. *J Immunol Methods*. 1983; 65: p. 55–63.